Single cell RNA sequencing reveals immunomodulatory mechanism of stem cell factor and granulocyte colony-stimulating factor treatment in the brains of aged APP/PS1 mice

Robert S. Gardner, Michele Kyle, Karen Hughes, Li-Ru Zhao*

Department of Neurosurgery, State University of New York Upstate Medical University, Syracuse, NY, 13210, USA

Running head: Immunomodulation in the brain of aged APP/PS1 mice by hematopoietic growth factors

***Corresponding author**:

Li-Ru Zhao, MD., PhD

Department of Neurosurgery

State University of New York Upstate Medical University

750 E. Adams Street

Syracuse, New York 13210. USA

E-mail: ZHAOL@upstate.edu

Telephone: +1 315 464 8470; Fax: +1 315 464 5504

Abstract

Alzheimer's disease (AD) leads to progressive neurodegeneration and dementia. AD primarily affects older adults with neuropathological changes including amyloid-beta (Aβ) deposition, neuroinflammation, and neurodegeneration. We have previously demonstrated that systemic treatment with stem cell factor (SCF) and granulocyte colony-stimulating factor (G-CSF) (SCF+G-CSF), reduces Aβ load, increases Aβ uptake by activated microglia and monocytes/macrophages (Mo/Mac), reduces neuroinflammation, and restores dendrites and synapses in the brains of aged APPswe/PS1dE9 (APP/PS1) mice. However, the mechanisms underlying SCF+G-CSF-enhanced brain repair in aged APP/PS1 mice remain unclear. This study used a transcriptomic approach to explore the mechanisms by which SCF+G-CSF treatment alters the functions of microglia and Mo/Mac in the brains of 28-month-old APP/PS1 mice. After 5-day injections of SCF+G-CSF, single-cell RNA sequencing was performed on $CD11b^+$ microglia and Mo/Mac isolated from the brain. Flow cytometry was used for identifying $CD11b^+$ microglia and Mo/Mac in the brain. Both transcriptional profiling and flow cytometry data demonstrated dramatic increases in the population of Mo/Mac in the brain following SCF+G-CSF treatment. SCF+G-CSF treatment robustly increased the transcription of genes implicated in activated immune cells, including gene sets that regulate inflammatory processes and cell migration. SCF+G-CSF treatment also increased a cell population co-expressing microglial and Mo/Mac marker genes. This cell cluster aligned with a disease-associated microglial profile linked with Aβ restriction and phagocytosis. S100a8 and S100a9 were the most robustly enhanced genes in both microglial and Mo/Mac clusters following SCF+G-CSF treatment. Furthermore, the topmost genes differentially expressed after SCF+G-CSF treatment were largely upregulated in S100a8/9-positive microglia and Mo/Mac, suggesting a largely well-conserved transcriptional profile related to SCF+G-CSF treatment in cerebral immune cells. This S100a8/9-associated transcriptional profile contained genes related to pro- and anti-inflammatory responses, neuroprotection, and Aβ plaque inhibition or clearance. This study sheds new light on the cellular and molecular mechanisms of SCF+G-CSF-mitigated AD neuropathology in the aged brain.

Keywords: Alzheimer's disease; Hematopoietic growth factors; Single-cell RNA sequencing; Microglia; Macrophages; S100a8/9

Background

Alzheimer's disease (AD) is the most prominent neurodegenerative disease and the leading cause of dementia [1, 2]. The primary risk factor for AD is advanced age. Strikingly, approximately one in nine Americans over the age of 65 is currently living with AD-related dementia. Moreover, societal impacts of AD are immense with annual healthcare costs greater than $320 billion [2]. Without novel effective treatments, the number of Americans afflicted with AD is projected to reach 13.8 million by 2060 [3].

Neuropathological hallmarks of AD include extracellular plaques composed of aggregated amyloid-beta (Aβ), intracellular neurofibrillary tangles composed of aggregated tau, and neuro-inflammation [4, 5]. Aβ peptides generated by sequential proteolysis of amyloid pre-curser protein (APP) by β- and γ-secretases are particularly prone to aggregation [6, 7], resulting in plaques that contribute to tau pathology, neuro-inflammation, synaptic dysfunction, neuro-degeneration, and cognitive decline [8, 9, 10, 11, 12, 13].

Several experiments crossing Aβ and tau transgenic animal models that develop extracellular plaques and intracellular tangles, respectively, revealed that while Aβ pathology enhanced the formation of neurofibrillary tangles, tau pathology had relatively little effect on Aβ deposits [14, 15, 16]. Injections of Aβ fragments, oligomers, or fibrils into the brain likewise are shown to enhance the formation of neurofibrillary tangles [17], also increasing neuro-inflammation and neuro-degeneration, and impairing spatial learning and memory [18, 19, 20]. These collective findings suggest that Aβ neuro-pathology is a contributory factor and relatively early event in the progression of AD, and that Aβ clearance is a promising focus for therapeutic advancements [21]. Indeed, clearance of Aβ from the brain is associated with mitigation of neuro-degeneration and cognition decline, largely observed in mouse models [22, 23, 24].

Nonetheless, currently approved and prescribed treatments for AD are primarily symptomatic, for example, targeting behavioral problems, rather than the underlying neuro-pathology, and thus, do not stop or reverse the progression of the disease [25]. The notable exception is Aducanumab, an anti-aggregated Aβ monoclonal antibody shown to reduce Aβ plaques [26]. Aducanumab has recently been approved by the United Stated Food and Drug

Administration for treatment of mild cognitive impairment and mild dementia in individuals presenting with Aβ pathology. However, high treatment costs, concerns over the therapeutic efficacy to treat cognitive impairment [27], and the incidence and severity of adverse events, e.g., amyloid-related imaging abnormalities, including brain micro-hemorrhage [28], suggest that the development of additional treatments remains imperative.

Microglia are the primary phagocytic cells in the brain, acting as the first line of immune defense, surveilling the microenvironment clearing debris or pathogens, including aggregated Aβ plaques [29], to maintain homeostasis [30]. In AD, bone marrow-derived blood monocytes augment the brain's immune cell population by migrating to the brain and differentiating into macrophages, also showing efficacy to uptake and degrade aggregated Aβ [31, 32, 33]. Notably, mutations in genes related to microglial and macrophage activation, for example, triggering receptor expressed on myeloid cells 2 (Trem2), a transmembrane receptor activated by Aβ [34] and associated with Aβ clearance [35, 36], confer relatively high risk of age-related or late-onset AD [37, 38], importantly linking immune system dysregulation to AD pathogenesis [39].

Microglia and macrophages that migrate to and surround Aβ plaques release a host of extra-cellular vesicles and soluble molecules, including cytokines with inflammatory and/or anti-inflammatory functions, and thus, additionally regulate neuro-inflammatory processes [40, 41]. Activated microglia and macrophages associated with a relatively anti-inflammatory profile are thought to confer debris clearance without significantly contributing to inflammation and may enhance angiogenesis and tissue repair [22, 42, 43, 44]. However, during the progression of AD pathology, microglia and macrophages increasingly take on a relatively pro-inflammatory state [45, 46, 47]. Although numerous reports demonstrate Aβ clearance is enhanced by pro-inflammatory signaling or cytokines [23, 48, 49, 50, 51], persistent or chronic inflammation is generally thought to enhance Aβ spreading and aggregation [52], creating a vicious cycle leading to neuro-degeneration [53]. Altogether, these findings strongly suggest that the development of novel AD therapies to clear Aβ from the brain, should likewise consider their effects on inflammation.

Stem cell factor (SCF) and granulocyte colony-stimulating factor (G-CSF), two hematopoietic growth factors, synergistically stimulate proliferation, differentiation, and mobilization of hematopoietic stem cells and progenitor cells, significantly increasing the population of blood leukocytes and augmenting the body's immune response [54,

55, 56, 57]. SCF and G-CSF also act directly on neurons, glia, and blood vessel cells [58, 59, 60], in the central nervous system. SCF and G-CSF treatment enhances angiogenesis, neural survival, neurite outgrowth, synaptogenesis, and neurogenesis, and reduces neuro-inflammation in several models of neurodegenerative diseases, neurological disorders, and brain trauma [61, 62, 63, 64, 65, 66, 67]. In AD patient populations, plasma levels of SCF and G-CSF are significantly reduced [68, 69]. Clinical studies have also demonstrated inverse correlations between SCF or G-CSF and AD severity [69, 70] and Aβ levels in cerebrospinal fluid [71].

Demonstrating the efficacy of SCF and G-CSF to treat AD neuropathology in pre-clinical studies, our lab has observed that systemic treatment of combined SCF and G-CSF (SCF+G-CSF) leads to long-lasting reductions of Aβ plaques in the hippocampus and cortex of middle-aged [72] and aged [22] APP/PS1 mice, a commonly used mouse model of Aβ pathology in AD research. Coincident with these findings, SCF+G-CSF treatment increases the association between Aβ plaques and activated Trem2^{+} microglia and macrophages, increases Aβ contained in CD68^{+} lysosomal compartments, increases the density of the anti-inflammatory marker IL-4, and decreases the density of the pro-inflammatory marker NOS-2 in the hippocampus and cortex of aged APP/PS1 mice [22]. These collective results suggest that SCF+G-CSF treatment enhances Aβ clearance by activating microglia and macrophages to uptake and degrade Aβ plaques, while also shifting the environment toward a relatively anti-inflammatory state. Importantly, these effects further correspond to SCF+G-CSF-mediated reductions of aggregated tau and increases in the dendritic marker MAP2^{+} and post-synaptic marker PSD-95, suggesting treatment-related rebuilding of neural connections. Thus, SCF+G-CSF treatment in aged APP/PS1 mice ameliorates or reverses each central feature of AD neuropathology: aggregated Aβ, aggregated tau, neuro-inflammation, and degeneration of neural processes and synaptic connections. Consistent results are reported in various models, e.g., [73, 74, 75].

These findings strongly indicate that SCF+G-CSF treatment changes the functions of microglia and macrophages to mitigate AD neuropathology in the aged brain. Leveraging a single-cell RNA sequencing approach, the aim of the present study is to identify novel transcriptional profiles of microglia and macrophages in the brain associated with SCF+G-CSF treatment in aged APP/PS1 mice. Similar approaches have been used to identify novel functional states of microglia related to AD, including a disease associated microglia (DAM) profile found to limit the progression of AD pathology [76, 77]. Here, we analyzed the transcriptional profiles of isolated CD11b^{+}

microglia and monocytes/macrophages (Mo/Mac) from the brains of aged APP/PS1 mice treated with SCF+G-CSF or vehicle solutions. The findings provide unbiased identification of distinct treatment-related transcriptional profiles of immune cells in the brain, which shed new light on the mechanisms underlying SCF+G-CSF-induced amelioration of neuropathology in the aged brain in the context of AD.

Methods

Animals

All methods were carried out in accordance with the National Institutes of Health Guide for the Care and Use of Laboratory Animals and approved by the State University of New York Upstate Medical University Institutional Animal Care and Use Committee. Aged APP/PS1 mice (male, 28 months old) (stock# 034832, Jackson Labs) were used in these experiments. APP/PS1 mice express both chimeric amyloid precursor protein (human APP695swe) with Swedish double mutations (K595N/M596L) and human presenilin protein 1 carrying the exon-9-deleted variant (PS1-dE9) [78]. APP/PS1 mice develop plaques of human amyloid beta (Aβ) peptide in the brain by 6-7 months of age. Mice had free access to food and water and were housed in a 12-hour light/dark cycle. The health status of the mice was checked daily.

Experimental Design

The experimental design is summarized in Figure 1. Twelve APP/PS1 mice at the age of 28-months old were subcutaneously injected with stem cell factor (SCF; 200 µg/kg in saline) and granulocyte colony-stimulating factor (G-CSF; 50 µg/kg in 5% dextrose) or an equal volume of vehicle solution (n=6 in each group) for five consecutive days. The next morning after completing the five injections, whole brains (3 mice in each group) were removed and dissociated. $CD11b^+$ cells were isolated using magnetic-activated cell sorting (MACS). The isolated $CD11b^+$ cells from the brains of 3 mice in the same treatment group were pooled together for single-cell RNA sequencing (scRNAseq). The isolated $CD11b^+$ cells were also analyzed using flow cytometry for immuno-phenotyping. Flow cytometry was performed on aliquots of the pooled $CD11b^+$ cells used for scRNAseq and on $CD11b^+$ cells of individual samples isolated from the brains of 6 additional mice (3 in each group).

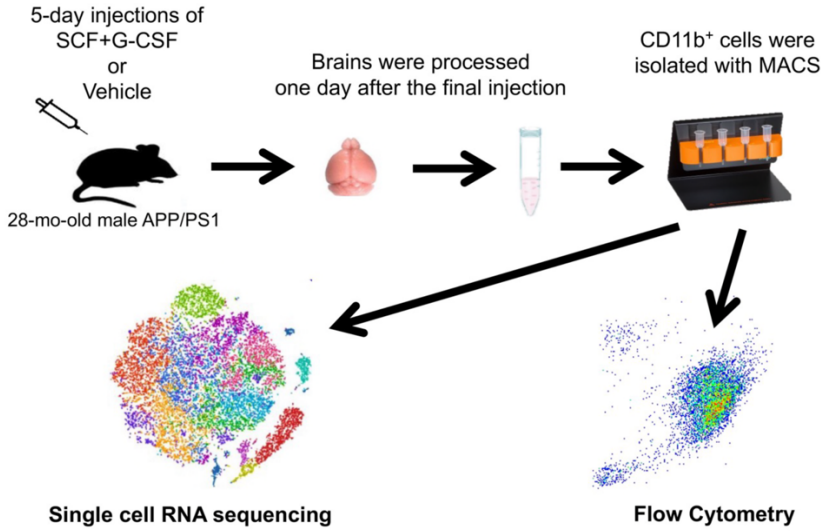

Fig. 1 Experimental flow chart. APP/PS1 mice (28-month-old; male) were subcutaneously injected with either combined stem cell factor (SCF) and granulocyte colony-stimulating factor (G-CSF) or vehicle solution for 5 days. The next day, the whole brains were excised and processed into single-cell suspensions. After debris and dead cells were removed, CD11b$^+$ microglia and monocytes/macrophages (Mo/Mac) were isolated using magnetic-activated cell sorting (MACS). The isolated CD11b$^+$ cells were used for either single-cell RNA sequencing or flow cytometry.

Cell processing and CD11b$^+$ isolation for single cell RNA sequencing and flow cytometry

Cell dissociation. Mice were anesthetized with Ketamine (100mg/kg) and Xylazine (10mg/kg) (i.p.) and euthanized by intracardiac perfusion with ice-cold heparinized (10k U / L; Sagent Pharm. 25021-403-04) Dulbecco's phosphate-buffered saline (D-PBS; 14190136; ThermoFisher). Each brain was removed, immersed in a cell culture dish containing ice-cold D-PBS+ (D-PBS supplemented with calcium, magnesium, glucose and pyruvate; 14287080; ThermoFisher), and minced (~1-2 mm in any dimension) using an ice-cold sterile scalpel blade. Brains were dissociated using the commercially-available Adult Brain Dissociation Kit (130-107-677; Miltenyi Biotec) and the Gentle MACS Octo Dissociator with Heaters (130-096-427; MB) according to manufacturer's specifications. Briefly, tissue pieces from each brain were transferred into a C-tube (130-096-334; Miltenyi Biotec) containing 1950 µL of enzyme mix 1. Enzyme mix 2 was subsequently added (30 µL), and the sample was dissociated using the program 37C_ABDK_01. Each sample was spun down, and the re-suspended pellet was passed through pre-wet 400 µM (43-50400-03; pluriSelect) and 70 µM cell filters (43-50070-51; pluriSelect). Each cell suspension was centrifuged at 300 x g for 10 min at 4°C, and the cell pellet was re-suspended in 3.1 mL D-PBS+ for subsequent processing to clear debris and dead cells.

Debris and dead cell removal. Debris removal solution (900 µL; 130-109-398; Miltenyi Biotec) was mixed into each suspension and 4 mL of D-PBS+ was layered over top. The samples were centrifuged at 3000 x g for 10 min at 4°C .The top and debris inter-phases were removed, and the remaining solution was diluted in D-PBS+ (14 mL), inverted three times, and centrifuged at 1000 x g for 10 min at 4°C. Dead and dying cells were removed using the Dead Cell Removal kit from Miltenyi Biotec (130-090-101). Briefly, the pellets were resuspended and incubated for 15 min at room temperature in 100 µL of the dead cell removal magnetically-labeled antibody. Binding Buffer (400 µL) was added to the suspension, which was subsequently passed through a pre-washed LS column (130-042-401; MB; 1 LS column per brain), placed in a strong magnetic field (Quadro MACS Separator,130-090-976, attached to the MACS MultiStand, 130-042-303; Miltenyi Biotec), and topped with a pre-wet 70 µM cell filter. Each filter/column was further washed 4 times with Binding Buffer. Flow-through, largely depleted of dead cells (confirmed by trypan blue staining of cell aliquots), was collected and centrifuged at 300 x g for 10 min at 4°C. Each pellet was resuspended in 1 mL 1X MACS buffer (130-091-376; Miltenyi Biotec; diluted in PBS) and passed through a 40 µM cell filter (43-50040-51; pluriSelect). Additional MACS buffer (4 mL) was passed through the 40 µM filter to maximize cell recovery. The suspension from each brain was centrifuged at 300 x g for 10 min at 4°C, and each pellet was resuspended in 270 µL MACS buffer prior to magnetic activated cell sorting of $CD11b^+$ brain cells.

Magnetic-activated cell sorting of $CD11b^+$ brain cells. CD11b ultra-pure micro beads (30 µL; 130-126-725; Miltenyi Biotec) were incubated with the sample for 15 min at 4°C. Subsequently, each cell suspension was washed with 2 mL MACS buffer and centrifuged at 300 x g for 10 min at 4°C. Each pellet was resuspended in 500 µL MACS buffer, and passed through a pre-washed LS column (1 LS column per brain) placed in the magnetic field. Each LS column was topped with a pre-wet 70 µM cell filter. Each filter/column was further washed 3 times with MACS buffer. To enhance CD11b purity, the magnetically-captured cells were eluted into a second LS column affixed to the magnet. The second LS column was washed 3 times with MACS buffer. Viability of magnetically-captured cells (eluted into a new tube away from the magnet) was assessed by trypan blue staining (1:2 dilution sample in trypan blue; BioRad 1450013). Cell viability was quantified as the proportion of cells that did not take up the dye. Aliquots were further processed for scRNAseq and for flow cytometry.

Single-cell RNA sequencing

The cell suspensions were centrifuged at 300 x g for 10 min at 4°C ,and the pellets were resuspended in DMEM/F12 (11320033; ThermoFisher) supplemented with Fetal Bovine Serum (10%) to achieve a concentration of 1000 cells / µL. The cell solutions were placed on ice and run for scRNAseq using the Chromium single cell gene expression platform (10× Genomics) to target 10,000 cells. Following manufacturer specifications (GEM Single Cell 3' Reagent Kit v3.1: 10x Genomics), samples and barcoded-oligonucleotide/primer-containing gel beads were loaded onto a G chip (1000127: 10x Genomics) and run on a Chromium Controller to partition single cells for subsequent generation of barcoded cDNA using reverse transcription. Pooled cDNA was sequenced using the Illumina NextSeq 500 High Output Kit. These steps were performed by the Molecular Analysis Core facility at Upstate Medical University.

Flow cytometry

Separate aliquots of cell suspensions used for scRNAseq were centrifuged at 300 x g for 10 min at 4°C, and the pellets were resuspended in D-PBS supplemented with 1% BSA. Aliquots (100 µL) were incubated with anti-mouse CD11b-APC (1:50 dilution; 130-113-802 Miltenyi Biotec) and anti-mouse CD45-PE (1:50 dilution; 130-110-797, Miltenyi Biotec) for 10 min at 4°C. Separate aliquots were incubated with control isotype antibodies. Cells were washed with 2 mL D-PBS (1% BSA) and centrifuged for 300 x g for 10 min at 4°C. The pellets were resuspended in 600 µL D-PBS (1% BSA) for flow cytometry analysis. Additional samples were stained and analyzed as above using the following modifications: the samples were blocked with FcR block (1:200 dilution; 553141, BD Biosciences) for 10 min at 4°C and incubated with anti-mouse CD11b-PE (1:50 dilution; 130-113-806, Miltenyi Biotec) and anti-mouse CD45-APC (1.15:100 dilution; 103112, Biolegend) for 15 and 30 min, respectively at 4°C. SCF+G-CSF-treated and vehicle-control samples were counterbalanced across all experiments. Cells were assayed on the BD LSR-II cytometer with FACSDiva software (BD Biosciences) using 561 nM and 633 nM excitation lasers paired with detection filters 585/15 nM and 630/20 nM for PE and APC signals, respectively.

Data analysis and statistics

Single cell RNA sequencing. Analysis and figure generation of scRNAseq data were primarily performed using Partek Flow software. Reads were trimmed and aligned to the mm10 assembly using Bowtie2. To ensure the results presented here were robust to choice of aligners, all primary findings were corroborated using alternate aligners, including STAR. To limit artifacts, unique molecular identifiers (UMIs) that identify individual transcripts were de-duplicated. Moreover, cell-specific barcodes were filtered to limit those not associated with a cell, using default parameters. A single cell count matrix was generated by quantifying the reads for each cell barcode to the mm10_refseq_v97 gene annotation model. Based on recommendations for using 10x genomics kits, the minimum read overlap for inclusion in the count matrix was set to 50% of read length. Strand specificity was set to Forward-Reverse. Low quality cells (e.g., doublets, those with few reads) were manually filtered out based on the distributions of read counts, detected genes, and ribosomal counts across the entire dataset. Manual filtering was done blindly with respect to treatment condition and individual gene profiles. This method yielded a total of 19,008 cells. Normalization was performed to account for differences in total UMI counts per cell and values were log2-transformed. To reduce noise and limit analysis of genes with little-to-no expression, genes with counts less than 1 in 99% of cells were excluded from analysis. Data were dimensionally reduced by Principal Component Analysis. One hundred components were computed and the ten explaining the most variance in the dataset were used to define clusters. Unsupervised cluster analysis was performed using the Louvain algorithm. t-Distributed stochastic neighbor embedding (tSNE) dimensional reduction plots were generated to visualize cell clusters and their associated gene expression profiles.

Select cluster identities were confirmed using the bioinformatics tool Cluster Identity Predictor [79]. This tool computes a cell class identity score based on gene expression overlap between an experimental dataset and reference immune cell dataset collated by the Immunological Genome Project [80]. Immune cell classes showing significant overlap with a given cluster were identified. Significant overlap was defined as an identity score greater than 1.96 standard deviations above the mean score across all cell classes examined.

To evaluate changes across treatment groups (SCF+G-CSF vs. Vehicle) in cell distributions across clusters, chi-square analysis was performed (Graph Pad v9) with alpha set to 0.05. Differentially expressed genes across conditions were identified using the Biomarker function in Partek. For restricted gene sets (e.g., homeostatic or

DAM gene sets), differentially expressed genes showing a ≥ 0.4 log2-fold change across conditions, with a false discovery rate (FDR)-adjusted (step-up method) p value < 0.05 [81] were highlighted as significant. For analyses across the entire transcriptome, significance thresholds were set to a ≥ log2-fold change across conditions with an FDR-adjusted p value < 0.01. This threshold limited significant hits to those genes most robustly altered by SCF+G-CSF treatment. The bioinformatics tool VolcaNoseR [82] was used to generate volcano plots of differentially expressed genes. Enriched gene ontologies, reactome pathways, and gene interaction networks (generated by querying the STRING database) were identified and analyzed using default settings in Cytoscape 3.9.1 [83, 84].

Flow Cytometry. Data processing was performed using Flow Jo v10. Debris was gated out using forward and side scatter profiles, and single cells were selected based on forward scatter area by forward scatter height (Figure 2A-B). Isotype-stained controls were used for thresholding and identification of $CD11b^+$ and $CD45^+$ cells. CD11b purity of the MACS-isolated samples was estimated as the percent of single cells positive for CD11b. $CD11b^+$ /$CD45^{high}$ populations were manually gated blind to treatment condition. Outcome measures and findings across treatment groups were robust to the use of distinct antibodies and fluorochromes. Thus, all flow cytometry data within each treatment group were combined for subsequent presentation and analysis. An independent samples t-test was performed (Graph Pad Prism v9) to compare the proportion of $CD11b^+$ cells contained in the $CD45^{high}$ gate across treatment groups with alpha set to 0.05.

Results

The isolated $CD11b^+$ cells show a high degree of purity and viability

To assess the purity of the MACS-isolated $CD11b^+$ cells from the brains of aged APP/PS1mice, flow cytometry was used to quantify the cells with cell surface expression of CD11b. We

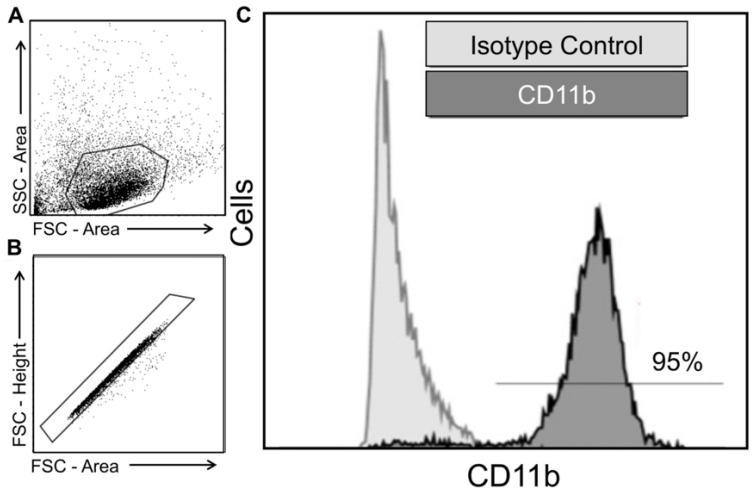

Fig. 2 MACS-isolated $CD11b^+$ cells show a high degree of purity. Gating strategies using forward scatter (FSC) and side scatter (SSC) profiles exclude (**A**) cell debris (**B**) cell multiplets from the MACS-isolated $CD11b^+$ cell suspension. (**C**) Representative data of flow cytometry. Relative to signal from isotype controls, ~95% of the single cells show expression for CD11b.

observed that 95% of the MACS-isolated cells expressed CD11b (Fig. 2C). The MACS-isolated CD11b$^+$ cells also showed a high degree of viability as assessed by trypan blue staining (95% viable). These findings indicate that our cell isolation method is effective, yielding highly pure and viable CD11b$^+$ cells isolated from the brains of aged APP/PS1 mice.

The vast majority of CD11b$^+$ cells isolated from the brain of aged APP/PS1 mice are microglia and monocytes/macrophages

Next**,** scRNAseq was performed on the MACS-isolated CD11b$^+$ cells from the brains of vehicle controls and SCF+G-CSF-treated old APP/PS1 mice. Gene transcription profiles were analyzed in a total of 19,008 cells, and tSNE plots were constructed to visualize expression patterns (Fig. 3). Unsupervised cluster analysis across all cells revealed 14 relatively unique clusters, which were color-coded and ranked according to cell count (Fig. 3A).

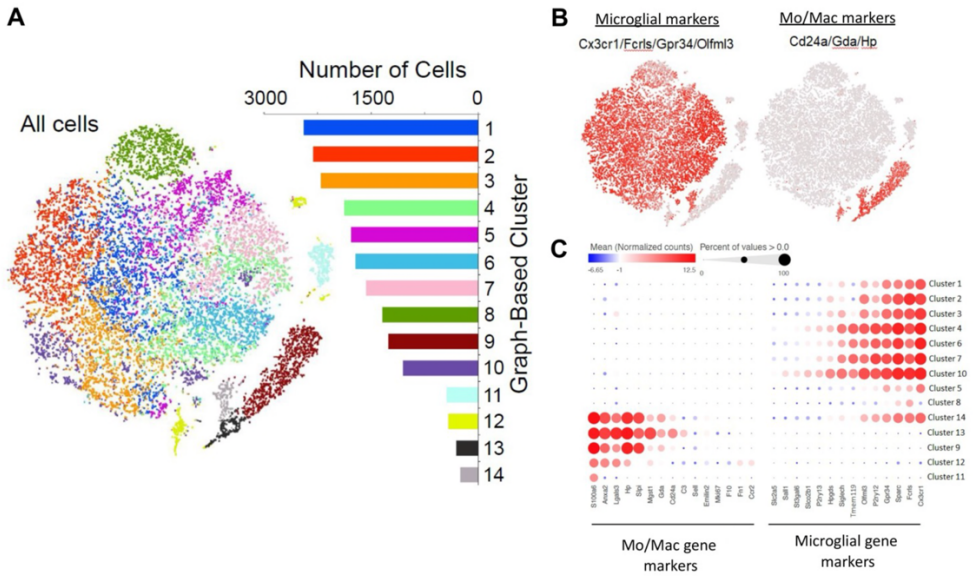

Fig. 3 Cluster analysis of the single-cell RNA sequencing dataset reveals 14 cell clusters largely differentiated by gene markers of microglia and Mo/Mac. (**A**) t-distributed stochastic neighbor embedding (tSNE) dimensionality reduction plots of 19,008 cells that are classified into 14 unique graph-based clusters defined and color-coded by unique transcriptional profiles. The number of cells in each cluster is shown in the corresponding bar graph. (**B**) Expression (in red) of microglial gene markers across tSNE plots indicates that the vast majority of clusters (1-8, 10, 14) associate with a microglia gene profile. Expression (in red) of Mo/Mac gene markers across tSNE plots indicates that several clusters (9, 12-14) associate with a Mo/Mac gene profile. Note, cluster 14 highly expresses genes associated with both microglia and Mo/Mac. (**C**) Clusters 1-8, and 10 show microglia but not Mo/Mac gene profiles, while clusters 9, 12, and 13 show Mo/Mac but not microglia profiles. Cluster 14 shows the expression of genes in both categories, while cluster 11 does not show the expression of genes in either category. Bubble plots: the diameters of the circles correspond to the percentage of cells that express a given gene, while the color intensities of the circles correspond to the magnitude of expression.

These clusters highly expressed numerous genes commonly used to identify CD11b$^+$ microglia and CD11b$^+$ monocytes/macrophages (Mo/Mac). Cst3, Lyz2, and Tyrobp (markers of microglia and Mo/Mac) showed relatively robust expression across individual clusters (Fig. S1) (Supplemental data File 1). In contrast, these clusters did not express gene markers of neurons, neuron progenitor cells, astrocytes, oligodendrocytes, oligodendrocyte progenitor cells, vascular cells, and fibroblasts (Fig. S1). These results confirm the purity of the MACS-isolated CD11b$^+$ cells and also reveal that the isolated CD11b$^+$ cells are primarily composed of microglia and Mo/Mac.

To further characterize the primary cell classes contained in each cluster, we analyzed the expression of gene sets identified by Haage et al. [85] to differentiate microglia from Mo/Mac. We found that the majority of clusters (clusters 1-8, and 10; containing 85.9% of all cells) aligned with microglia gene profiles (Cx3cr1$^+$, Fcrls$^+$, Sparc$^+$, Gpr34$^+$, P2ry12$^+$, Olfml3$^+$, Tmem119$^+$, Siglech$^+$, Hpgds$^+$, P2ry13$^+$, Slco2b1$^+$, St3gal6$^+$, Sall1$^+$, and Scl2a5$^+$) but not Mo/Mac profiles (S100a6$^+$, Anxa2$^+$, Lgals3, Hp$^+$, Slpl$^+$, Mgst1$^+$, Gda$^+$, CD24a$^+$, C3$^+$, Sell$^+$, Emilin2$^+$, Mki67$^+$, F10$^+$, Fn1$^+$, and Ccr2$^+$) (Fig. 3B-C; Fig. S2). Thus, clusters 1-8, and 10 were classified as microglia. In stark contrast, gene profiles of clusters 9, 12, and 13 (containing 11.8% of cells) largely aligned with those of Mo/Mac but not microglia (Fig. 3B-C). Thus, clusters 9, 12, and 13 were classified as Mo/Mac. Consistent with this classification, as compared to clusters 1-8 and 10, clusters 9, 12, and 13 showed significantly higher expression of Lgals3 (Fig. 3C; Fig. S2), which is an additional proposed marker gene of Mo/Mac following their migration to the brain [86]. Differential expression analysis largely confirmed findings across clusters. Expression levels of microglial marker genes were significantly enriched in clusters 1-8, and 10, whereas the expression levels of Mo/Mac marker genes were significantly enriched in clusters 9, 12-13 (all p values < 0.0001; Fig. S2).

Cluster 14 (containing 1.3% of cells) is a unique cluster showing robust expression of both microglial and Mo/Mac marker genes (Fig. 3C). Subsequent analysis of cluster 14 demonstrated significant expressions of S100a6, Anxa2, Hp, Lgals3, Slpi, and Gda (all Mo/Mac markers) in Cx3cr1$^+$, P2ry12$^+$, Fcrls$^+$, Gpr34$^+$, and Sparc$^+$ cells (Table S1). These findings strongly suggest robust co-expression of Mo/Mac and microglial gene sets in a small group of CD11b$^+$ cells. To further probe the primary cell identity of cluster 14, we cross-referenced its genome-wide expression profile with those in collated immune cell reference datasets [80] and evaluated overlap with microglia

and Mo/Mac. We observed that cluster 14 showed relatively robust overlap with Mo/Mac profiles relative to microglia (Supplemental Data File 2).

While cluster 11 (containing 2.3% of cells) showed high expression of S100a6, very little expression was observed of the remaining microglial and Mo/Mac gene markers (Fig. 3C). Inspection of gene sets associated with additional immune cell classes revealed relatively high expressions of Cd3d, Cd8b1, and Cd8a (Fig. S1), demonstrating a profile consistent with that of $CD11b^+$ T-cells [87]. Confirming this result, cluster 11 gene profiles primarily aligned with those of T-cells in reference datasets (Supplemental Data File 2).

Altogether, these findings suggest that the $CD11b^+$ cells isolated from the brains of aged APP/PS1 mice are overwhelmingly microglia, but also include a modest population of Mo/Mac, a small population of cells that co-express both microglial and Mo/Mac gene markers, and a small population of T-cells. Given prior findings that SCF+G-CSF treatment induces changes in microglia and Mo/Mac to engulf Aβ [22], the current study focuses strictly on microglia and Mo/Mac clusters.

Microglial clusters lie across a gradient of transcriptional profiles largely associated with activation and disease states

Differential gene analysis across cell clusters revealed gene sets relatively unique to each cluster. Across the microglial clusters, many top differentially expressed genes (DEG) were associated with homeostatic (e.g., Tmem119, P2ry12) or reactive disease states (e.g., Apoe, Cst7, Trem2, Itgax, Lpl, and Clec7a) [88], [89]. Emerging evidence demonstrates a role of highly reactive disease-associated microglia (DAM) [76] in slowing the progression of AD pathology [89]). Moreover, DAM can take on distinct inflammatory profiles that correspond to phagocytic efficacies [90].

To better understand the diversity of microglial clusters (1-8, and 10), we probed expression patterns of curated gene sets linked to homeostatic and DAM profiles [88] as well as those in inflammatory marker genes. Homeostatic and disease-associated microglial marker genes were variably expressed and generally demarcated the microglial

clusters (Fig. 4). Homeostatic genes (e.g., Tmem119, P2ry12, Glul) were robustly enriched in clusters 4, 6, and 7, coinciding with a reduction of DAM genes (e.g., Lpl, Fabp5, Clec7a, Cst7). This observation suggests a relatively homeostatic hub of microglia (clusters 4, 6, 7). Homeostatic genes, however, were downregulated in clusters 1, 2, 3, 5, and 8, which appeared to represent distinct DAM profiles. Clusters 5 and 8 showed modest expression of lysosomal marker gene Cd68 and increased expression in relatively few variably-expressed DAM genes (e.g., Cst7 and Fabp5). In contrast, clusters 1, 2, and 3 displayed heightened expression of Cd68 and the DAM genes Lyz2, Cst7, Clec7a, Fabp5, Spp1, Lpl, Itgax, Apoe, and Csf1, suggesting advanced or later-stage DAM. Cluster 3 also expressed relatively high levels of Nfkbiz, Tnf, and Il1b genes, showing an inflammatory profile.

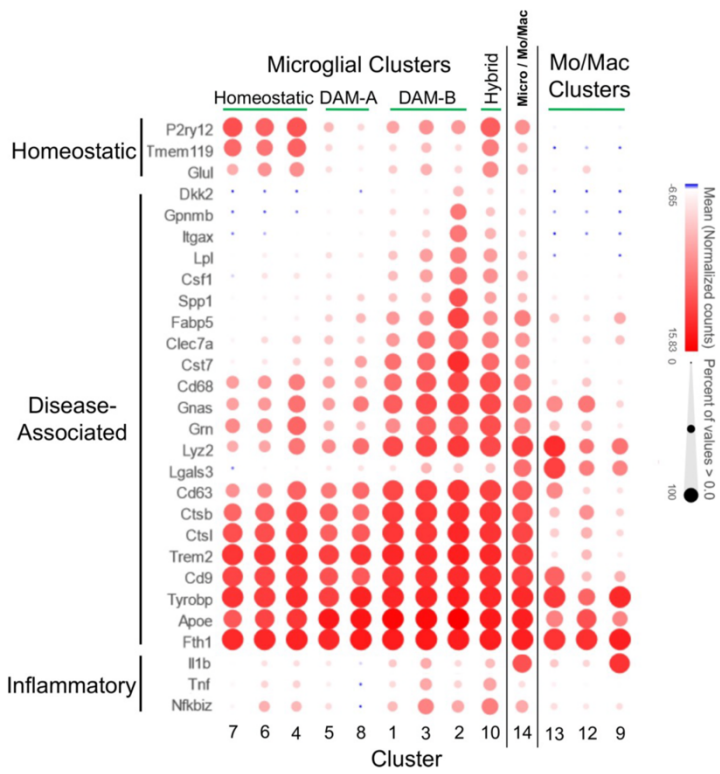

Fig. 4 Expression profiles of homeostatic and DAM gene sets reveal a gradient of activation states across clusters. Expression of gene sets linked to homeostatic microglia, disease associated microglia (DAM), and inflammation are plotted across cell clusters 1-8 and 10. Homeostatic gene markers (e.g. Tmem119, P2ry12) are highly expressed in clusters 4, 6, and 7, while these clusters show relatively little expression of DAM gene markers (e.g., Itgax, clec7a, Cst7, Lpl, Fabp5), suggesting that CD11b^{+} cells in these cell clusters are homeostatic microglia. In contrast, microglial cell clusters 1, 2, 3, 5, and 8 show high expression DAM genes with relatively little expression of homeostatic genes. These clusters are classified as DAM-A (clusters 5 and 8) and DAM-B (clusters 1, 2, 3) according to the extent of expression across most of DAM genes. Note, cluster 10 is associated with both homeostatic and DAM gene profiles and is characterized as a hybrid microglia cluster. Similar to the microglial clusters, Mo/Mac clusters (9, 12, and 13) also highly express Tyrobp, Apoe, and Fth1 genes, but these Mo/Mac clusters additionally show increased expression of Lgals3 and decreased expression of most DAM genes. Cluster 14 aligns with a Mo/Mac profile, but cells in this cluster also express genes consistent with DAM-B microglia. Bubble plots: the diameters of the circles correspond to the percentage of cells that express a given gene, while the color intensities of the circles correspond to the magnitude of expression.

Microglial cluster 10 showed robust expression of the majority of DAM and homeostatic marker genes (Fig. 4). This profile was confirmed in individual Tmem119^{+} and P2ry12^{+} microglia (Table S2), suggesting co-expression of DAM and homeostatic marker genes in a subset of microglia. This cluster additionally showed relatively high expression levels of inflammatory genes (Nfkbiz, Tnf, and Il1b), collectively identifying a population of microglia characterized by high levels of homeostatic genes, DAM signature genes, and inflammatory genes.

Most broadly, the transcriptional profiles across microglia clusters found here, appear to represent a wide range of transitional states, that, with the exception of a small subset of microglia (cluster 10), highlight an inverse relationship between homeostatic and DAM gene expression. For subsequent analysis, the clusters were grouped into 4 distinct hubs (Fig. 4): 1) a relatively homeostatic hub (clusters 4, 6, and 7), 2) a relatively reactive hub with modestly enriched DAM signature genes (clusters 5 and 8; characterized as DAM-A), 3) a hub relatively enriched with a high degree of DAM signature genes (clusters 1, 2, and 3; characterized as DAM-B), and 4) a hybrid hub enriched with both homeostatic and DAM gene profiles (cluster 10). While we observed between-cluster and intra-cluster variation, our cluster hub classification reflects robust changes in the transcriptional profiles of cluster-specific marker genes (Fig. 4).

Cluster 14, which aligned with both microglial and Mo/Mac gene profiles, highly expressed several genes associated with DAM-B microglia (e.g., Trem2, Cd68, Cst7, Clec7a, Fabp5). While Mo/Mac clusters also expressed high levels of DAM genes, including Fth1, Tyrobp, and Apoe, the Mo/Mac clusters displayed large increases in the Mo/Mac and DAM marker gene Lgals3 and showed little expression of the remaining DAM genes, including Trem2 (Fig. 4).

SCF+G-CSF treatment increases the proportion of Mo/Mac in the brains of aged APP/PS1 mice

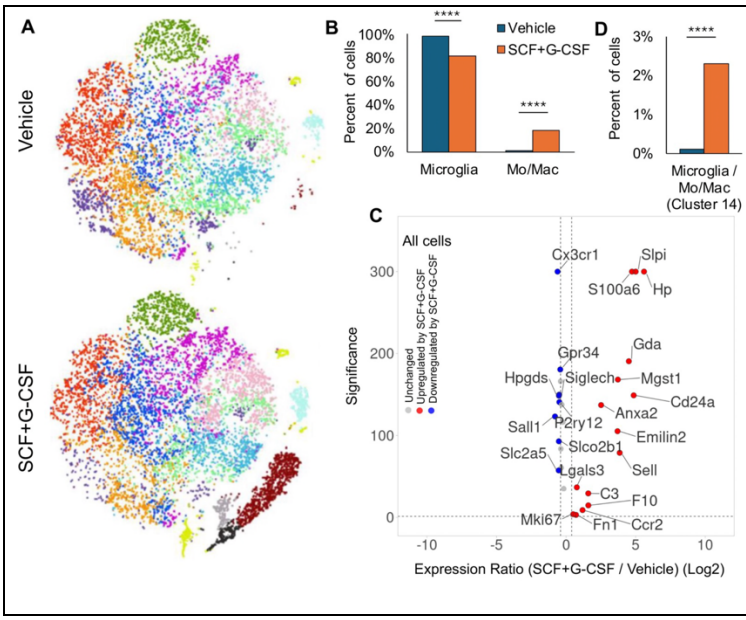

Fig. 5 SCF+G-CSF treatment alters the distribution of cells across clusters, augmenting the prevalence of Mo/Mac in the brains of aged APP/PS1 mice. (**A**) t-distributed stochastic neighbor embedding (tSNE) dimensionality reduction plots of cells separated by treatment. (**B**) SCF+G-CSF treatment shifts the distribution of CD11b$^+$ cells with reduced microglial cells and increased Mo/Mac in the brains of APP/PS1 mice. **** $p < 0.0001$. (**C**) A volcano plot highlights microglial and Mo/Mac gene sets that are largely changed by SCF+G-CSF treatment. Genes upregulated by SCF+G-CSF treatment are shown in red. Genes downregulated by SCF+G-CSF treatment are shown in blue. False discovery rate-corrected p values (-log10) are shown on the y-axis. The log2-transformed expression ratios are computed as expression levels in the SCF+G-CSF-treated mice compared to those in the vehicle control group and are plotted on the x-axis. Dotted lines indicate significance thresholds. The top 20 genes differentially expressed are labeled. (**D**) SCF+G-CSF treatment increases the number of cluster 14 cells that highly express both microglia and Mo/Mac gene sets. **** $p < 0.0001$.

Next, we sought to determine whether SCF+G-CSF treatment alters the proportions of microglia and Mo/Mac in the brains of aged APP/PS1 mice. Figure 5A shows t-SNE plots for visualizing cell clusters in vehicle control and SCF+G-CSF treatment. In the vehicle controls, 98.7% of the cells were contained in the microglial clusters (clusters 1-8, 10), and 1.3% in the Mo/Mac clusters (clusters 9, 12, 13) (Fig. 5B; Fig. S3). Cell distributions in the SCF+G-CSF-treated mice were significantly shifted with a smaller percent of cells in the microglial clusters (79.9% of cells; $p < 0.0001$) and a larger percent in the Mo/Mac clusters (20.1% of cells; $p < 0.0001$) than that of the vehicle controls (Fig. 5B; Fig. S3). Strikingly, cells from the SCF+G-CSF-treated mice accounted for 95.3% (range across clusters: 82% – 99%) of the cells contained in the Mo/Mac clusters (9, 12, 13; Fig. S3B). In line with these findings, expression levels of all Mo/Mac gene markers were significantly upregulated by SCF+G-CSF treatment (Fig. 5C). These findings suggest that SCF+G-CSF treatment dramatically enhances the recruitment of Mo/Mac into the brains of aged APP/PS1 mice. We also observed that cluster 14 cells, which highly co-expressed microglial and Mo/Mac gene profiles, were almost exclusively (96.4%) from SCF+G-CSF-treated mice (Fig. 5D). These results suggest that SCF+G-CSF treatment induces Mo/Mac to take on transcriptional profiles of microglia and/or induces microglia to take on Mo/Mac profiles.

To validate the scRNAseq data which suggest that SCF+G-CSF treatment enhances the population of Mo/Mac in the brain, we measured the cell surface expression of CD11b and CD45 using flow cytometry in separate aliquots of MACS-isolated $CD11b^{+}$ cells. Previous studies show that the expression profiles of these proteins can be used to differentiate Mo/Mac from microglia in the brain, with Mo/Mac aligning with a $CD45^{high}$ profile [91, 92]. We found that SCF+G-CSF treatment significantly increased the proportion of $CD45^{high}/CD11b^{+}$ cells in the brains of aged APP/PS1 mice compared to the vehicle controls ($p < 0.05$;

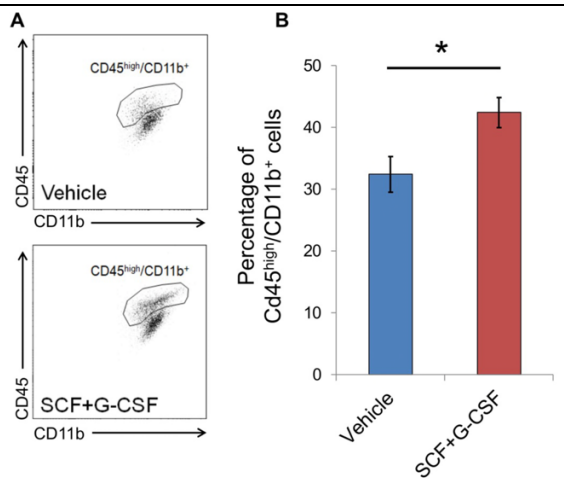

Fig. 6 SCF+G-CSF treatment augments the recruitment of Mo/Mac into the brains of aged APP/PS1 mice as confirmed by flow cytometry. (**A**) Representative flow cytometry dot plot graphs showing the population of $CD45^{high}/CD11b^{+}$ Mo/Mac in the brains of aged APP/PS1 mice treated with or without SCF+G-CSF. (**B**) SCF+G-CSF treatment increases the percentage of $CD45^{high}/CD11b^{+}$ Mo/Mac in the brains of aged APP/PS1 mice. Data are presented as mean ± SEM. * $p < 0.05$. T-test, n = 4.

Fig. 6). These data fully support the scRNAseq findings that SCF+G-CSF treatment increases the population of Mo/Mac in the brains of aged APP/PS1 mice.

SCF+G-CSF treatment changes CD11b$^+$ cell activation states in the brains of aged APP/PS1 mice

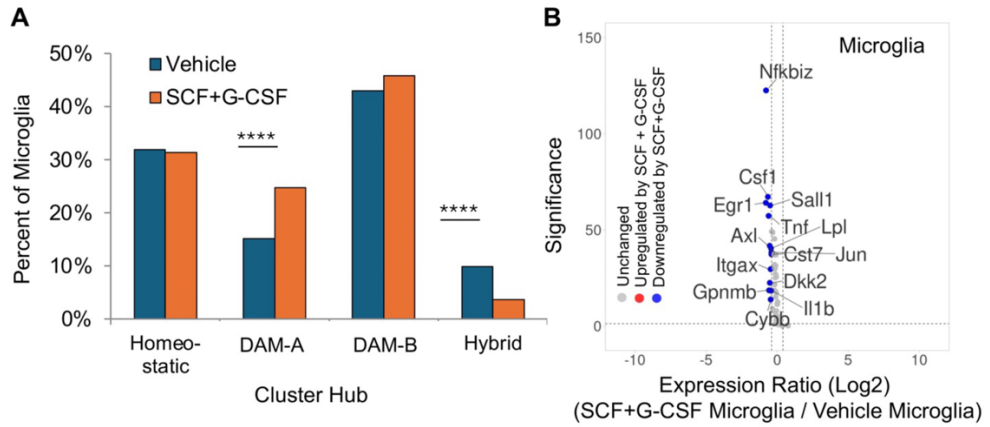

Fig. 7 SCF+G-CSF treatment alters the reactive profiles of microglia. (**A**) SCF+G-CSF treatment increases the percentage of microglia in the DAM-A hub and reduces the percentage of cells in the hybrid hub (cluster 10). **** $p < 0.0001$. (**B**) A volcano plot highlights homeostatic, DAM, and inflammatory gene sets that are significantly changed by SCF+G-CS treatment in microglial clusters pooled together (1-8, 10). Genes upregulated by SCF+G-CSF treatment are shown in red. Genes downregulated by SCF+G-CSF treatment are shown in blue. False discovery rate-corrected p values (-log10) are shown on the y-axis. The log2-transformed expression ratios are computed as expression levels in the SCF+G-CSF-treated mice relative to those in the vehicle control group. The log2-transformed expression ratios are plotted on the x-axis. Dotted lines indicate significance thresholds.

We next assessed the effects of SCF+G-CSF treatment in modifying the activation profiles in CD11b$^+$ microglia. Restricting analysis to microglia clusters, SCF+G-CSF treatment significantly increased the percentage of microglia contained in the DAM-A hub ($p < 0.0001$, Fig. 7A) and decreased the number of microglia in the inflammatory hybrid homeostatic/DAM hub ($p < 0.0001$, Fig. 7A) (hybrid cluster 10, Fig. 4). The proportions of microglia contained in the homeostatic hub and DAM-B hub were not changed by SCF+G-CSF treatment (Fig. 7A). These results suggest a shift away from inflammatory and homeostatic microglial profiles following SCF+G-CSF treatment. Consistent with these findings, differential expression analysis across all microglial clusters revealed that SCF+G-CSF treatment reduced the expression of inflammatory markers (e.g. Nfkbiz, Tnf, Il1b; Fig. 7B). However, SCF+G-CSF treatment also reduced the expressions of gene sets typically upregulated in DAM (e.g., Csf1, Axl, Itgax) as well as those typically downregulated in DAM (e.g., Egr1, Sall1, Jun; Fig. 7B), suggesting a variable or nuanced modification of transcriptional response by SCF+G-CSF treatment in DAM gene sets.

Transcriptome-wide responses to SCF+G-CSF treatment are largely comparable across microglia and Mo/Mac in the brains of aged APP/PS1 mice

Next, we performed transcriptome-wide differential gene analysis across experimental groups for unbiased identification of transcriptional changes in microglia and Mo/Mac following SCF+G-CSF treatment. We first identified genes altered by SCF+G-CSF treatment in all cell clusters. We observed that the vast majority of differentially expressed genes (DEGs) were upregulated (n = 359 genes) by SCF+G-CSF treatment, rather than downregulated (n = 34 genes). The top 10 DEGs ranked by significance and the number of differentially-expressed transcripts (Fig. 8A) included four genes of the calcium-binding S100a family (S100a8, S100a9, S100a6, S100a11), the lipocalin family gene (Lcn2), the anti-inflammatory annexin A1 (Anxa1), the hemoglobin-binding haptoglobin (Hp), the anti-viral interferon-induced transmembrane gene (Ifitm1), the resistin-like molecule (Retnlg), and the whey acidic protein/four-disulfide core domain 21 (Wfdc21). These 10 genes were all upregulated by SCF+G-CSF treatment. This gene set collectively plays a prominent role in immune cell activation, such as microglial cell- and Mo/Mac-mediated inflammation and phagocytosis, and cell migration. Gene set enrichment analysis corroborated these findings linking the DEGs with immune responses, inflammatory responses, stress responses, and leukocyte migration (Fig. S4; Supplemental Data File 4).

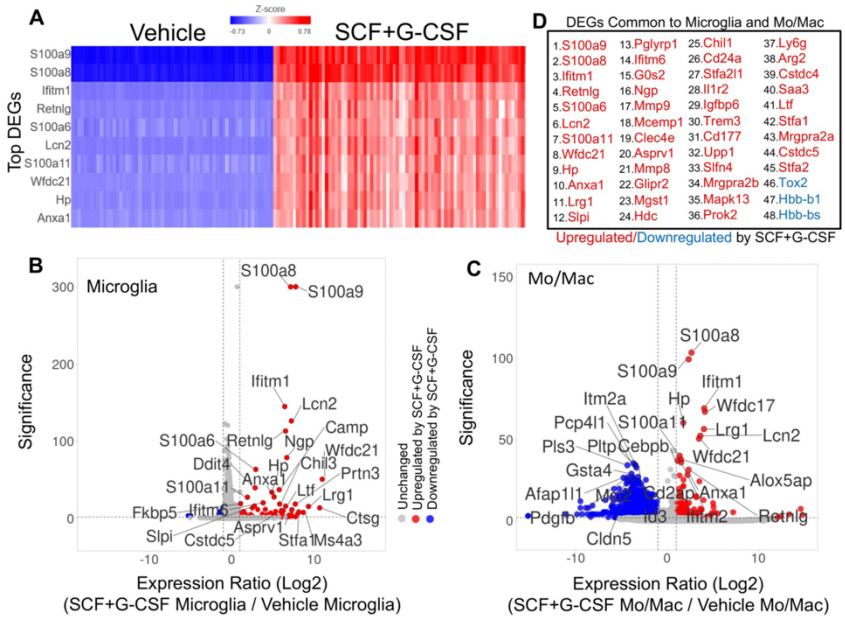

Fig. 8 Transcriptome-wide responses to SCF+G-CSF treatment in microglia and Mo/Mac. (**A**) A hierarchical clustering heat map illustrates the top 10 differentially expressed genes that are upregulated (in red) across all cells by SCF+G-CSF treatment. Among the SCF+G-CSF-upregulated genes, S100a8 and S100a9 are the highest upregulated genes. (**B** and **C**) Volcano plots highlight genes differentially expressed by SCF+G-CSF treatment in microglial clusters (**B**) and in Mo/Mac clusters (**C**). Genes upregulated by SCF+G-CSF treatment are shown in red. Genes downregulated by SCF+G-CSF treatment are shown in blue. In microglia, 70 genes are upregulated, and 18 genes are downregulated by SCF+G-CSF. In Mo/Mac, 133 genes are upregulated, and 2637 genes are downregulated by SCF+G-CSF. False discovery rate-corrected *p* values (-log10) are shown on the y-axis. The log2-transformed expression ratios are computed as expression levels in SCF+G-CSF-treated mice relative to those in the vehicle control group. The log2-transformed expression ratios are plotted on the x-axis. Dotted lines indicate inclusion thresholds: ≥ 2-fold change, and FDR-corrected *p* value < 0.01. Note, *p* values are restricted to 300 decimal places. The top 25 genes differentially expressed are labeled. (**D**) A list of genes differentially expressed (≥ 2-fold change, FDR-corrected *p* value < 0.01) by SCF+G-CSF treatment are common to both microglia and Mo/Mac. Genes are ordered from lowest to highest FDR-correct *p* values in the entire dataset.

The topmost genes upregulated by SCF+G-CSF treatment were largely comparable across microglial (Fig. 8B) and Mo/Mac (Fig. 8C) clusters and across homeostatic and DAM-associated microglial cluster hubs (Fig. S5). These findings identify a stable transcriptional response following SCF+G-CSF treatment in various cell classes. Expression profiles across individual cell clusters for the top 25 genes upregulated by SCF+G-CSF treatment are presented in Figure S6. Overlapping genes (n = 48) prominently altered by SCF+G-CSF treatment in both microglia and Mo/Mac (Supplemental Data File 3) are presented in Figure 8D.

While many of the DEGs upregulated by SCF+G-CSF treatment showed robust effects across microglia and Mo/Mac, we also noted differences across microglia and Mo/Mac transcriptional profiles in response to SCF+G-CSF treatment. For example, while the majority of DEGs prominently altered by SCF+G-CSF treatment in microglia were upregulated (n = 70 genes) rather than downregulated (n = 18 genes), in Mo/Mac, 133 genes were upregulated, and 2637 genes were downregulated (Fig. 8B-C). These results suggest a more extensive transcriptional response to SCF+G-CSF treatment in the Mo/Mac. Of note, the topmost genes downregulated by SCF+G-CSF in Mo/Mac included those associated with actin remodeling, cell adhesion and migration (e.g., Cd2ap, Pls3, Myo10, Afap1l1), vascular integrity (e.g., Pdgfb, Cldn5), and lymphocyte activation (e.g., Itm2a, Cd2ap).

S100a8 and S100a9 are robustly expressed in microglia and Mo/Mac of the brain in aged APP/PS1 mice following SCF+G-CSF treatment

Overall, the most striking effect following SCG+G-CSF treatment was upregulation of the genes S100a8 and S100a9. As S100a8 and S100a9 correlate with and interact directly with Aβ plaques, and they both are highly expressed in microglia and macrophages that surround plaques [93], [94], we further probed S100a8 and S100a9 expression profiles in our dataset. Violin density plots show the distributions of S100a8^{+}, S100a9^{+}, and S100a8/9-negative microglia and Mo/Mac in vehicle control and SCF+G-CSF treatment groups (Fig. 9). The vast majority of the CD11b^{+}cells that highly expressed S100a8 or S100a9 were observed in the SCF+G-CSF-treated mice.

To ensure that SCF+G-CSF treatment upregulated S100a8 and S100a9 (S100a8/9) gene expression in microglia rather than in small subsets of Mo/Mac contained in the microglial clusters, we probed the expression levels of microglial gene markers in S100a8/9-positive cells and S100a8/9-negative cells. In microglia clusters, S100a8/9-

positive cells co-expressed several specific gene markers of microglia, including Tmem119, at comparable levels to those in S100a8/9-negative cells (Fig. S7). This observation reveals that SCF+GCSF treatment robustly enhances S100a8/9 gene expressions in microglia.

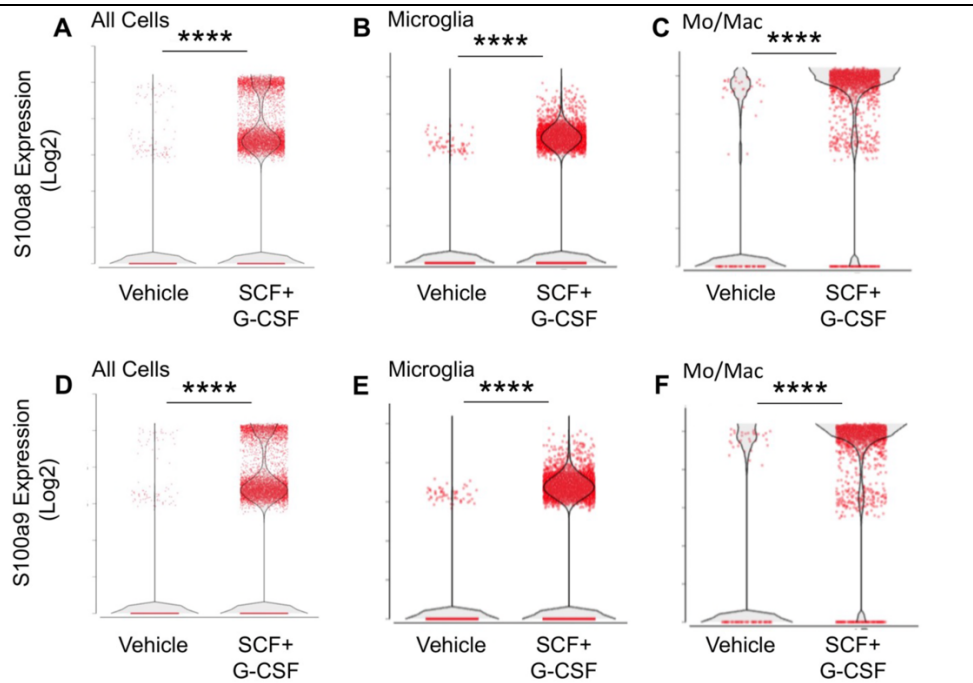

Fig. 9 S100a8 and S100a9 genes are robustly upregulated by SCF+G+CSF treatment and most highly expressed in Mo/Mac. Violin density plots show that S100a8 (**A-C**) and S100a9 (**D-F**) are significantly upregulated by SCF+G-CSF treatment in cells across all clusters (**A** and **D**), in microglial clusters (**B** and **E**), and in Mo/Mac clusters (**C** and **F**). Individual cells are shown as red dots. **** $p < 0.0001$.

Interestingly, the topmost genes upregulated with SCF+G-CSF treatment in the entire dataset were co-expressed and upregulated in the S100a8/9-positive microglia compared to the S100a8/9-negative microglia as well as in the S100a8/9-positive Mo/Mac compared to S100a8/9-negative Mo/Mac (Fig. S8). These findings suggest that S100a8 and S100a9 are reliable marker genes associated with the prominent transcriptional responses to SCF+G-CSF treatment in microglia and Mo/Mac in the brains of aged APP/PS1 mice.

Network analysis of DEGs across experimental groups identifies highly inter-connected "hub" genes functionally connected to S100a8/9 expression

To identify potential interactions among the genes altered by SCF+G-CSF treatment, we constructed a functional network of gene-gene interactions among treatment-related DEGs (Fig. 10). A central hub within the network

contained several of the top DEGs, including S100a8/9. Within this hub, we also noted highly inter-connected genes, including Il1b, Mmp9, Mpo, Cd44, and Rac2 (Fig. 10B). These findings suggest that central functions of SCF+G-CSF treatment are associated with inflammation-like activation (Il1b, Mpo, Cd44), and cell motility and remodeling (Mmp9, Rac2, Cd44).

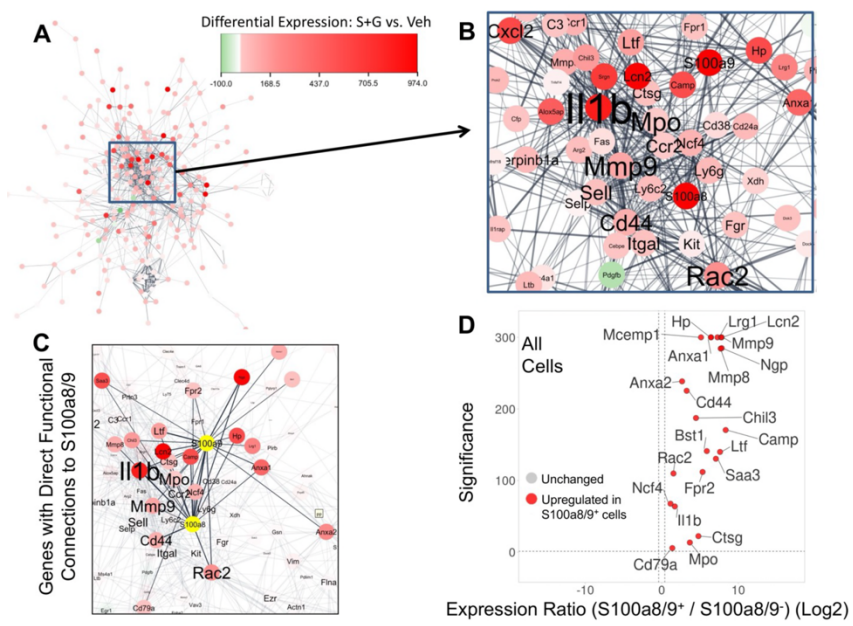

Fig. 10 Functional network of genes differentially expressed by SCF+G-CSF treatment reveals highly inter-connected "hub" genes and those functionally linked with S100a8 and S100a9. (**A**) The genes differentially expressed by SCF+G-CSF treatment in all cells were used to create a functional gene-gene interaction network by using the STRING database. Each node corresponds to a gene differentially expressed by SCF+G-CSF treatment. The edges (or links) between the nodes correspond to confirmed or potential functional connections. The color of the node corresponds to the intensity of differential expression, with red color indicating upregulation by SCF+G-CSF treatment. (**B**) A central hub of genes includes several of the top upregulated genes with SCF+G-CSF treatment (e.g., S100a8, S100a9, Anxa1, Lcn2, Hp). The size of the gene font corresponds to the extent of its connectivity in the network, identifying highly inter-connected "hub" genes, including Il1b, Mmp9, Rac2, and Cd44. (**C**) The 22 genes (Anxa1, Anxa2, Bst1, Camp, Cd44, Cd79a, Chil3, Ctsg, Fpr2, Hp, Il1b, Lcn2, Lrg1, Ltf, Mcemp1, Mmp8, Mmp9, Mpo, Ncf4, Ngp, Rac2, and Saa3) directly connected to S100a8 and S100a9 (S100a8/9) are highlighted. (**D**) This S100a8/9-linked gene set identified by network analysis is largely co-expressed and dramatically upregulated in individual S100a8/9-positive cells as shown in the single-cell RNA sequencing dataset. Genes upregulated in S100a8/9-positive cells are shown in red. False discovery rate-corrected *p* values (-log10) are shown on the y-axis. The log2-transformed expression ratios are computed as expression levels in S100a8/9-positive cells relative to those in S100a8/9-negative cells and are plotted on the x-axis. Dotted lines indicate significance thresholds. Note, *p* values are restricted to 300 decimal places.

Twenty-two genes (Anxa1, Anxa2, Bst1, Camp, Cd44, Cd79a, Chil3, Ctsg, Fpr2, Hp, Il1b, Lcn2, Lrg1, Ltf, Mcemp1, Mmp8, Mmp9, Mpo, Ncf4, Ngp, Rac2, and Saa3) upregulated by SCF+G-CSF treatment were directly connected to S100a8/9 (Fig. 10C), indicating direct functional interactions between S100a8/9 and the additional genes modified by SCF+G-CSF treatment. Importantly, S100a8/9-positive cells showed enriched expressions of all 22 of the SCF+G-CSF-upregulated genes (Fig. 10D), and the SCF+G-CSF-upregulated genes were also found in both the S100a8/9-positive microglia (Fig. S9A) and Mo/Mac (Fig. S9B). Interestingly, while the hub gene Il1b was upregulated by SCF+G-CSF treatment overall and in S100a8/9-positive Mo/Mac, it was not changed in S100a8/9-positive microglia (Fig. S9A). These findings demonstrate select contributions of S100a8/9-positive Mo/Mac to SCF+G-CSF-increased inflammatory hub gene Il1b.

Gene set enrichment analysis of S100a8/9-connected genes identified by network analysis showed enriched functions related to immune responses, inflammation (Cd44, Saa3, Anxa1, Il1b, Fpr2, Hp, Camp, S100a8, S100a9, Bst1, Mmp8), and leukocyte migration (Mmp9, Anxa1, Il1b, Rac2, Fpr2, Bst1, S100a8, S100a9) (Fig. S10). These findings are consistent with gene set enrichment analyses run on all DEGs (Fig. S4). Additionally, enriched reactome pathways included degradation of the extracellular matrix (Mmp9, Mmp8, Ctsg, Cd44), implicating a contributory mechanism for cell motility following SCF+G-CSF treatment. A complete list of enriched biological processes and reactome pathways is provided in Supplemental Data File 4.

Discussion

Our previous study demonstrated that SCF+G-SCF treatment activates microglia and Mo/Mac to engulf and clear Aβ, an effect associated with reduced neuroinflammation and reconstructed neural connections in the brains of 26-27-month-old APP/PS1 mice [22]. In the present study, we employed a transcriptome-wide analysis of $CD11b^+$ microglia and $CD11b^+$ Mo/Mac in the brains of 28-month-old APP/PS1 mice at the single-cell level following systemic treatment with SCF+G-CSF. The findings of this current study show that SCF+G-CSF treatment 1) modestly alters DAM transcriptional profiles, 2) increases the proportions of Mo/Mac in the brain, and 3) enhances transcriptional responses in microglia and Mo/Mac with increased expression of S100a8 and S100a9 and increased regulation of immune cell activation, migration, inflammation-like activation, and Aβ clearance. These findings reveal new cellular and molecular mechanisms by which SCF+G-SCF treatment modulates brain immune cells to reverse or mitigate neuropathology in the context of AD in old age.

In the current study, cluster analysis of MASC-isolated $CD11b^+$ cells from the brains of aged APP/PS1 mice identifies cell clusters with transcriptional profiles that aligned with microglia and Mo/Mac. The majority of these cell clusters (9 individual clusters: ~86% of all cells) align with the transcriptional profile of microglia. This observation is consistent with previous studies showing that the vast majority of $CD11b^+$ brain cells are microglia that comprise numerous transcriptionally-heterogeneous sub-populations in the aged, injured, or AD brain [95, 96], [97, 98, 99].

In the microglial clusters, we found high cluster-to-cluster variability in the expression of homeostatic (Tmem119, P2ry12) and DAM-associated genes (e.g., Cst7, Trem2, Itgax, Lpl, and Clec7a). We also observed that between-cluster transcriptional variability in microglia was largely characterized by an inverse relationship between homeostatic and DAM gene expression. This finding is well aligned with other reports showing transcriptional heterogeneity of microglia in AD that reflects transitionary stages from a homeostatic to a highly reactive DAM phenotype [76, 99].

The findings of this present study also show that SCF+G-CSF treatment increases the proportion of microglia with a DAM subset marked by little homeostatic gene expression (most notably P2ry12). Homeostatic gene expression has been shown to inversely correlate with the proximity of microglia to Aβ plaques. A microglial phenotype characterized by reductions of P2ry12 has been found next to Aβ plaques in autopsy brain tissue from AD patients [100]. Moreover, our earlier study has shown that P2ry12 expression is reduced in subsets of microglia that closely associate with Aβ plaques following SCF+G-CSF treatment [22]. Thus, our findings are consistent with an effect of SCF+G-CSF to augment a subset of DAM that closely surrounds Aβ plaques in the brains of aged APP/PS1 mice.

Additionally, we observed that SCF+G-CSF treatment reduces pro-inflammatory gene markers (e.g., Il1b and Tnf) in the microglial clusters. Reductions in pro-inflammatory genes, including Il1b, in DAM are associated with enhanced phagocytosis of Aβ [90]. Taken together, the DAM transcriptional profiles reported here, increased by SCF+G-CSF treatment, may reflect increases in a subset of highly phagocytic but relatively less inflammatory microglia surrounding Aβ plaques. These effects may contribute to reductions in Aβ burden and neuroinflammation in aged APP/PS1 mice [22].

The findings of the present study show that SCF+G-CSF treatment dramatically increases the numbers of Mo/Mac in the brains of aged APP/PS1 mice. The vast majority of $CD11b^{+}$ cells contained in Mo/Mac clusters are seen in the aged APP/PS1 mice treated with SCF+G-CSF, a finding confirmed by immunophenotyping using flow cytometry. Increased recruitment of Mo/Mac in the brain following SCF+G-CSF treatment has been reported in

middle-aged APP/PS1 mice [72]. These collective findings provide strong evidence for SCF+G-CSF-enhanced recruitment of Mo/Mac into the brains of the APP/PS1 mice even in advanced age.

Notably, SCF+G-CSF treatment increases the population of cells in a relatively small cluster (cluster 14) that aligned with both microglia and Mo/Mac gene sets. This finding suggests that SCF+G-CSF treatment may change the transcriptional profiles from one cell class to the other cell class. We found that the transcriptome in this cell cluster showed greater overlap with Mo/Mac reference datasets than with microglia datasets and included robust expression of the Mo/Mac marker Lgals3 [86]. Our findings also open the possibility that a subset of Mo/Mac that migrates to the brain following SCF+G-CSF treatment takes on a microglia transcriptional profile. This interpretation is in line with prior findings showing the expression of genes thought to be specific to microglia in Mo/Mac after they migrate to the brain [101]. As cluster 14 aligns with a DAM-associated profile (Trem2, Cst7, Csf1, Fabp5, and Clec7a), our findings also suggest the possibility that the recruited Mo/Mac may supplement DAM functions in the brain of aged APP/PS1 mice following SCF+G-CSF treatment.

In the remaining Mo/Mac clusters, the expression of DAM genes was relatively distinct from those in microglia. DAM marker gene expression in these Mo/Mac clusters was characterized by low expression of Trem2, yet high expression of its intracellular targets Tyrobp and Apoe. It has been reported that Tyrobp overexpression coupled with upregulation of downstream Apoe in Iba1^{+} microglia and macrophages is shown to reduce Aβ densities, and that both Trem2^{+} and Trem2-negative Tyrobp^{+}/Apoe^{+} microglia and macrophages can engulf Aβ plaques [102]. Therefore, it is plausible that a subset of Mo/Mac with high expression of Tyrobp and Apoe and low expression of Trem2 could be responsible for clearing Aβ in the brains of aged APP/PS1 mice. Interestingly, it has been proposed that a Tyrobp^{+}/Apoe^{+}/Trem2^{-} profile represents a transitional stage in the DAM progression of Iba1^{+} microglia. This transitional profile includes upregulation of Fth1, Lyz2, Apoe, and Tyrobp [103][76]. Thus, in the dataset of this present study, the Trem2^{low} Mo/Mac clusters that highly express Fth1, Lyz2, Apoe, and Tyrobp may reflect transitional stages toward a DAM-like phenotype associated with Aβ uptake. These observations are consistent with our previous findings that Mo/Mac that migrate to the brain following SCF+G-CSF surround Aβ plaques and correspond to Aβ clearance in APP/PS1 mice [72]. Most broadly, our findings are in agreement with extensive

studies suggesting a prominent role of Mo/Mac in mitigating Aβ pathology in AD [31, 32, 33] and strongly suggest a contributory role for Mo/Mac in SCF+G-CSF-induced clearance of brain Aβ in the aged brain of APP/PS1 mice.

Transcriptome-wide analysis in the present study reveals dramatic and robust effects of SCF+G-CSF treatment in augmenting gene sets linked with increased immune responses, including inflammation and leukocyte migration. The top genes upregulated by SCF+G-CSF treatment (e.g., S100a8, S100a9, Ifitm1, Lcn2, Mmp9) are prominently associated with highly activated microglia and Mo/Mac, inflammation, and cell migration to sites of injury [93], [104–109]. Network analysis has confirmed these effects by identifying hub genes that are functionally related to cell movement and remodeling (Mmp9, Rac2, Cd44), and inflammation (Il1b, Mpo, Cd44).

S100a8 and S100a9 were observed as the two most robustly upregulated genes following SCF+G-CSF treatment. Moreover, S100a8/9-positive microglia and Mo/Mac highly co-express the topmost upregulated genes. These findings suggest that SCF+G-CSF treatment leads to a conserved or fundamental transcriptional profile which is characterized by upregulation of S100a8/9-positive microglia and S100a8/9-positive Mo/Mac.

S100a family genes encode calcium-binding proteins that regulate fundamental intracellular processes, including intracellular calcium homeostasis, and cytoskeleton rearrangement. S100a8 and S100a9 are the most prominent calcium-binding proteins in bone marrow-derived phagocytic cells, and the secretion of S100a8 and S100a9 is associated with inflammatory processes [104, 110, 111]. Cytoskeletal remodeling during periods of inflammation appears intertwined with, and a pre-requisite of, cell migration. S100a9 activity is essential for trans-endothelial migration of leukocytes [104, 112].

S100a8/9 are linked to disease states, including AD. S100a8/9 are enriched in the brains and sera of AD patients and are thought to contribute to AD pathogenesis by promoting neuroinflammation and Aβ aggregation [93,104,113]. Thus, we are largely surprised to find that S100a8/9 are the topmost upregulated genes following SCF+G-CSF treatment which has therapeutic effects to mitigate Aβ plaque load and induce anti-inflammatory effects centrally in aged APP/PS1 mice.

However, relevant to our findings, inflammation and Aβ plaque load enhance S100a8/9 transcription and secretion by surrounding microglia and macrophages [93, 94]. Therefore, the finding that SCF+G-CSF treatment increases the numbers of activated microglia and Mo/Mac that engulf Aβ plaques [22, 72] is consistent with SCF+G-CSF treatment-related enhancement of S100a8/9 transcription.

Despite the prevailing view that S100a8/9 induces neuro-inflammation and contributes to AD pathogenesis, several lines of research point to S100a9-induced reductions in neural toxicity and inflammation caused by Aβ. Recent evidence demonstrates that while S100a9 accelerates Aβ plaque formation, it also infiltrates and compacts Aβ plaques and sequesters toxic soluble Aβ species, resulting in mitigation of neural toxicity [114]. Co-aggregation of S100a9 with Aβ also reduces both S100a9 inflammation and Aβ cytotoxicity [115], suggesting the inflammatory role of S100a9 is conditional on its molecular interactions or conformational state. Consistent with this interpretation, while secreted S100a8/9 can form a heterodimer to activate toll-like receptors to induce inflammation [104], high levels of extracellular calcium induce the formation of S100a8/9 heterotetramers, which may act through distinct pathways and reduce the inflammatory tone [116]. These findings are consistent with anti-inflammatory properties of S100a8/9 under certain conditions, such as, combatting peripheral tissue damage during periods of heightened inflammation through sequestering the inflammatory cytokines Il1b and Tnf, [104]. In the dataset of this current study, SCF+G-CSF treatment shows downregulation of Il1b and Tnf in microglia and robust upregulation of S100a8/9, suggesting a key role for S100a8/9 in modulating inflammatory signaling in aged APP/PS1 mice, in part by sequestration of select inflammatory cytokines.

While it remains possible that enhanced pro-inflammatory cytokines may contribute to phagocytic clearance of Aβ [23, 48, 49, 50, 51], inflammatory processes associated with S100a8/9 may be mitigated by anti-inflammatory genes co-upregulated by SCF+G-CSF treatment in microglia and Mo/Mac. Several genes that are highly co-expressed in S100a8/9-positive microglia and S100a8/9-positive Mo/Mac or functionally linked with S100a8/9 expression (e.g., Anxa1, Anxa2, Chil3, Hp, Lrg1, Ngp, and Wfdc17) have been shown to confer anti-inflammatory or alternatively activated properties [118, 119, 120, 121, 122, 123, 124, 125, 126], which are associated with tissue repair [40, 44, 127].

Moreover, several of the genes (Anxa1, Anxa2, Fpr2, S100a6, S100a11, Mmp9, Hp, Il1b) robustly upregulated with SCF+G-CSF and linked with S100a8/9 are also associated with Aβ clearance and/or neuroprotection. These genes and their roles in AD and neuroprotection are briefly outlined below.

Annexins are calcium- and phospholipid-binding proteins. Microglia Anxa1 mediates non-inflammatory phagocytosis of apoptotic cells. Under inflammatory conditions, Anxa1 treatment restores non-inflammatory clearance of apoptotic, but not healthy, neurons, and promotes the reduction of inflammatory processes in reactive microglia *in vitro* [126]. Anxa1 is upregulated in microglia that surround Aβ plaques in AD patients and AD mouse models [128]. Moreover, exogenous Anxa1 treatment *in vitro* enhances Aβ phagocytosis by microglia and reduces Aβ-stimulated transcription of pro-inflammatory genes, including Tnf in microglia [128]. In young 5xFAD mice, Anxa1 treatment reduces Tnf, mitigates blood-brain barrier pathology, and increases synaptic densities [129], demonstrating a neuroprotective role in AD pathology. The effects of Anxa1 in Aβ clearance are largely mediated by activation of its Fpr1/2 receptor [128]. Notably, our findings reveal that both Anxa1 and Fpr2 are also upregulated with SCF+G-CSF treatment. Moreover, an S100a11-encoded Anxa1 adapter protein enhances cytosolic and membrane-associated levels of Anxa1, which likewise confers neural protection in cerebral ischemia [130]. A similar anti-inflammatory and neuroprotective role of Anxa2 is reported in a TBI study [124].

S100a6 binds calcium and zinc and is found in cells that surround Aβ plaques. In a study targeting the contribution of zinc to Aβ aggregation, S100a6 treatment-reduced Aβ plaques in the brains of 22-month-old APP/PS1 mice were thought to reflect the ability of S100a6 to sequester excess zinc [131].

Hp encodes haptoglobin which is prominently identified as a hemoglobin-binding protein. The scavenging effects of haptoglobin in preventing neurotoxicity in the brain have been demonstrated in the condition of sub-arachnoid hemorrhage [132]. As cerebral micro-bleeds are associated with AD and correlate with Aβ burden [133], SCF+G-CSF-increased Hp expression may mitigate neuropathology in aged APP/PS1 mice. As shown in an *in vitro* study, haptoglobin associates with Aβ plaques to inhibit the formation of Aβ fibrils [134], suggesting direct functions of Hp to oppose Aβ deposition. High mobility group box-1 (HMGB1) is an initiator and activator of neuroinflammatory responses. HMGB1 inhibits microglial Aβ clearance, and factors that bind HMGB1 reduce Aβ

load and supress neuroinflammatory [135, 136]. Notably, it has been shown that haptoglobin also binds and sequesters HMGB1 and that haptoglobin treatment sequesters HMGB1, which leads to reductions in tissue loss and pro-inflammatory TNF and increases in anti-inflammatory IL-10 in microglia and macrophages in a mouse model of stroke [125].

Mmp9 is a zinc- and calcium-dependent endopeptidase. Through its proteolytic functions, Mmp9 plays a key role in the remodeling of the extracellular matrix, cell migration, and neuroplasticity [137]. Levels of Mmp9 are increased in AD, and Mmp9 shows the ability to degrade Aβ plaques [138, 139]. Moreover, neuronal over-expression of Mmp9 in 5xFAD mice shifts APP processing away from β- and γ-secretase pathways and toward an α-secretase pathway, which coincides with enhanced presynaptic densities [140]. An α-secretase pathway generates soluble APP-α, a non-amyloidogenic peptide that is reduced in AD and that promotes neuroprotection [141, 142].

Il1b, a classic pro-inflammatory cytokine, is associated with Aβ clearance. Overexpression of Il1b in the hippocampus of APP/PS1 mice reduces Aβ plaques, increases Iba1^{+} microglia and macrophage densities, and increases phagocytosis of Aβ [50, 51]. The findings of the present study show that SCF+G-CSF treatment increases Il1b expression in Mo/Mac, while SCF+G-CSF reduces Il1b in microglia. It remains unclear if macrophage-derived Il1b upregulated by SCF+G-CSF treatment plays a dominant role in enhancing phagocytic functions of CD11b^{+} macrophages to remove Aβ plaques.

Many of the genes upregulated by SCF+G-CSF treatment are activated by or modulate the concentrations of calcium, zinc, and/or iron (e.g., S100a8, S100a9, S100a11, S100a6, Lcn2, Hp, Mmp8, Mmp9, Anxa1, Anxa2, Fth1, Ltf). Indeed, metal sequestration and response to metal ions are enriched biological processes and reactome pathways that are associated with SCF+G-CSF treatment in this study. As increased levels of metal ions play a causal role in AD pathogenesis [143, 144], the findings of this study support further research into metal sequestration functions following SCF+G-CSF treatment in the context of AD.

While future studies are needed to determine whether the gene sets outlined here play causal roles in resolving AD pathology in advanced age, we note that the robust transcriptional changes induced by SCF+G-CSF treatment

remarkably overlap with those in CD11b$^+$ cells in the brain during a period of functional recovery in a mouse model of TDP-43 proteinopathy [145]. It remains to be determined whether this gene set upregulated by SCF+G-CSF could serve as a reliable transcriptional profile of recovery and brain repair in the context of AD.

There are several limitations of this study. Microglia and Mo/Mac populations were distinguished in our datasets based on known collated gene sets and reference transcriptome-wide datasets shown to differentiate the two cell classes [85]. If the advanced age and genotype of APP/PS1 mice or SCF+G-CSF treatment altered the transcriptional profiles of a significant number of cell type marker genes, our cell type classifications may be limited. While several myeloid cell classes have been shown to infiltrate the brains of transgenic mouse models of AD [146, 147], given findings that Mo/Mac are the primary myeloid cell population in the AD brain [31, 148], and those showing a dramatic and selective influx of Mo/Mac to the brain following SCF+G-CSF treatment in middle-aged APP/PS1 mice [72], the classification of infiltrated myeloid cells primarily as Mo/Mac following SCF+G-CSF treatment in the present study appears valid.

In the current study we evaluated brain-wide transcriptional changes following SCF+G-CSF treatment, precluding our ability to detect regional distinctions. As AD pathologies in the brain are spatially-diverse [149], it is possible that our study did not uncover SCF+G-CSF treatment effects limited to select brain regions.

We stress that this scRNAseq study was run on pooled samples of three APP/PS1 mice treated with SCF+G-CSF and three APP/PS1 mice injected with vehicle solution. Thus, we were unable to distinguish the contributions of individual samples to the transcriptional profile associated with each condition, and consequently, could not determine individual variability across mice. While sample variability in individual transcriptional profiles could contribute to small changes across groups, large effects highlighted in our transcriptome-wide analysis were remarkably consistent in the vast majority of cluster hubs. Thus, individual animal variability did not likely confound or drive our primary findings or conclusions.

In conclusion, the findings of this scRNAseq study reveal several potential cellular and molecular mechanisms by which combined systemic SCF+G-CSF treatment modulates the functions of Mo/Mac and microglia to clear and

degrade Aβ plaques and mitigate AD pathology in the APP/PS1 mouse brain in advanced age. Gene sets linked to immune cell activation, cell migration, and pro-inflammatory and anti-inflammatory processes are prominently enriched by the SCF+G-CSF treatment. Future studies will help clarify the causal role of these mechanisms in brain repair following SCF+G-CSF treatment in age-related AD.

List of abbreviations

Aβ	Amyloid-beta
AD	Alzheimer's disease
DAM	Disease associated microglia
DEGs	Differentially expressed genes
D-PBS	Dulbecco's phosphate-buffered saline
FDR	False discovery rate
G-CSF	Granulocyte colony-stimulating factor
MACS	Magnetic-activated cell sorting
Mo/Mac	Monocytes/macrophages
scRNAseq	Single-cell RNA sequencing
SCF	Stem cell factor
TBI	Traumatic brain injury
tSNE	t-Distributed stochastic neighbor embedding
UMIs	Unique molecular identifiers

Author Contributions: Conceptualization, L.R.Z.; methodology, R.G., M.K., and K.H.; formal analysis, R.G.; investigation, R.G.; resources, L.R.Z.; data curation, R.G.; writing—first draft preparation, R.G.; writing—review and editing, L.R.Z.; proofreading, M.K. and K.H.; visualization, R.G.; supervision, L.R.Z.; project administration and funding acquisition, L.R.Z. All authors read and approved the final version of the manuscript.

Funding: This study was supported by the National Institute on Aging of the National Institutes of Health in the United States (R01AG051674).

Availability of data and materials: The datasets generated during the current study are available from the corresponding author on reasonable request.

Declarations

Ethics approval and consent to participate: This study was approved by Animal Care and Use Committee of SUNY Upstate Medical University.

Concent for publication: Not applicable.

Competing interests: The authors declare no competing interests.

References

1. Armstrong R. Risk factors for Alzheimer's disease. Folia Neuropathol. 2019;57:87–105.

2. 2022 Alzheimer's disease facts and figures. [cited 2022 Nov 19]; Available from: https://alz-journals.onlinelibrary.wiley.com/doi/10.1002/alz.12638

3. Rajan KB, Weuve J, Barnes LL, McAninch EA, Wilson RS, Evans DA. Population estimate of people with clinical Alzheimer's disease and mild cognitive impairment in the United States (2020-2060). Alzheimers Dement J Alzheimers Assoc. 2021;17:1966–75.

4. Goedert M. Alzheimer's and Parkinson's diseases: The prion concept in relation to assembled Aβ, tau, and α-synuclein. Science. 2015;349:1255555.

5. Tiwari S, Atluri V, Kaushik A, Yndart A, Nair M. Alzheimer's disease: pathogenesis, diagnostics, and therapeutics. Int J Nanomedicine. 2019;14:5541–54.

6. O'Brien RJ, Wong PC. Amyloid Precursor Protein Processing and Alzheimer's Disease. Annu Rev Neurosci. 2011;34:185–204.

7. Seeman P, Seeman N. Alzheimer's disease: β-amyloid plaque formation in human brain. Synap N Y N. 2011;65:1289–97.

8. Fein JA, Sokolow S, Miller CA, Vinters HV, Yang F, Cole GM, et al. Co-localization of amyloid beta and tau pathology in Alzheimer's disease synaptosomes. Am J Pathol. 2008;172:1683–92.

9. Hanseeuw BJ, Betensky RA, Jacobs HIL, Schultz AP, Sepulcre J, Becker JA, et al. Association of Amyloid and Tau With Cognition in Preclinical Alzheimer Disease: A Longitudinal Study. JAMA Neurol. 2019;76:915–24.

10. Heneka MT, Carson MJ, El Khoury J, Landreth GE, Brosseron F, Feinstein DL, et al. Neuroinflammation in Alzheimer's disease. Lancet Neurol. 2015;14:388–405.

11. Mormino EC, Kluth JT, Madison CM, Rabinovici GD, Baker SL, Miller BL, et al. Episodic memory loss is related to hippocampal-mediated beta-amyloid deposition in elderly subjects. Brain J Neurol. 2009;132:1310–23.

12. Sato C, Barthélemy NR, Mawuenyega KG, Patterson BW, Gordon BA, Jockel-Balsarotti J, et al. Tau Kinetics in Neurons and the Human Central Nervous System. Neuron. 2018;97:1284-1298.e7.

13. Villemagne VL, Burnham S, Bourgeat P, Brown B, Ellis KA, Salvado O, et al. Amyloid β deposition, neurodegeneration, and cognitive decline in sporadic Alzheimer's disease: a prospective cohort study. Lancet Neurol. 2013;12:357–67.

14. Bloom GS. Amyloid-β and Tau: The Trigger and Bullet in Alzheimer Disease Pathogenesis. JAMA Neurol. 2014;71:505–8.

15. Hurtado DE, Molina-Porcel L, Iba M, Aboagye AK, Paul SM, Trojanowski JQ, et al. A{beta} accelerates the spatiotemporal progression of tau pathology and augments tau amyloidosis in an Alzheimer mouse model. Am J Pathol. 2010;177:1977–88.

16. Lewis J, Dickson DW, Lin WL, Chisholm L, Corral A, Jones G, et al. Enhanced neurofibrillary degeneration in transgenic mice expressing mutant tau and APP. Science. 2001;293:1487–91.

17. Götz J, Chen F, van Dorpe J, Nitsch RM. Formation of neurofibrillary tangles in P301l tau transgenic mice induced by Abeta 42 fibrils. Science. 2001;293:1491–5.

18. Diaz A, Limon D, Chávez R, Zenteno E, Guevara J. Aβ25-35 injection into the temporal cortex induces chronic inflammation that contributes to neurodegeneration and spatial memory impairment in rats. J Alzheimers Dis JAD. 2012;30:505–22.

19. Faucher P, Mons N, Micheau J, Louis C, Beracochea DJ. Hippocampal Injections of Oligomeric Amyloid β-peptide (1–42) Induce Selective Working Memory Deficits and Long-lasting Alterations of ERK Signaling Pathway. Front Aging Neurosci. 2016;7:245.

20. Henriques A, Jégo P, Farrugia C, Callizot N. Intra-hippocampal injections of Aβ oligomers induce cognitive impairments associated with neurodegeneration and activation of microglia in senescent mice: Characterization of a novel animal model of Alzheimer's disease. Alzheimers Dement. 2021;17:e054250.

21. Cai Z, Hussain MD, Yan L-J. Microglia, neuroinflammation, and beta-amyloid protein in Alzheimer's disease. Int J Neurosci. 2014;124:307–21.

22. Guo X, Liu Y, Morgan D, Zhao L-R. Reparative Effects of Stem Cell Factor and Granulocyte Colony-Stimulating Factor in Aged APP/PS1 Mice. Aging Dis. 2020;11:1423–43.

23. He Z, Yang Y, Xing Z, Zuo Z, Wang R, Gu H, et al. Intraperitoneal injection of IFN-γ restores microglial autophagy, promotes amyloid-β clearance and improves cognition in APP/PS1 mice. Cell Death Dis. 2020;11:440.

24. Tian D-Y, Cheng Y, Zhuang Z-Q, He C-Y, Pan Q-G, Tang M-Z, et al. Physiological clearance of amyloid-beta by the kidney and its therapeutic potential for Alzheimer's disease. Mol Psychiatry. 2021;26:6074–82.

25. Briggs R, Kennelly SP, O'Neill D. Drug treatments in Alzheimer's disease. Clin Med. 2016;16:247–53.

26. Sevigny J, Chiao P, Bussière T, Weinreb PH, Williams L, Maier M, et al. The antibody aducanumab reduces Aβ plaques in Alzheimer's disease. Nature. 2016;537:50–6.

27. Knopman DS, Jones DT, Greicius MD. Failure to demonstrate efficacy of aducanumab: An analysis of the EMERGE and ENGAGE trials as reported by Biogen, December 2019. Alzheimers Dement J Alzheimers Assoc. 2021;17:696–701.

28. Haeberlein S, Aisen PS, Barkhof F, Chalkias S, Chen T, Cohen S, et al. Two Randomized Phase 3 Studies of Aducanumab in Early Alzheimer's Disease. J Prev Alzheimers Dis. 2022;9:197–210.

29. Lee CYD, Landreth GE. The role of microglia in amyloid clearance from the AD brain. J Neural Transm Vienna Austria 1996. 2010;117:949–60.

30. Kettenmann H, Hanisch U-K, Noda M, Verkhratsky A. Physiology of microglia. Physiol Rev. 2011;91:461–553.

31. Simard AR, Soulet D, Gowing G, Julien J-P, Rivest S. Bone marrow-derived microglia play a critical role in restricting senile plaque formation in Alzheimer's disease. Neuron. 2006;49:489–502.

32. Town T, Laouar Y, Pittenger C, Mori T, Szekely CA, Tan J, et al. Blocking TGF-beta-Smad2/3 innate immune signaling mitigates Alzheimer-like pathology. Nat Med. 2008;14:681–7.

33. Yong VW, Rivest S. Taking Advantage of the Systemic Immune System to Cure Brain Diseases. Neuron. 2009;64:55–60.

34. Zhao Y, Wu X, Li X, Jiang L-L, Gui X, Liu Y, et al. TREM2 is a receptor for β-amyloid which mediates microglial function. Neuron. 2018;97:1023-1031.e7.

35. Fan Y, Ma Y, Huang W, Cheng X, Gao N, Li G, et al. Up-regulation of TREM2 accelerates the reduction of amyloid deposits and promotes neuronal regeneration in the hippocampus of amyloid beta1-42 injected mice. J Chem Neuroanat. 2019;97:71–9.

36. Wang Y, Cella M, Mallinson K, Ulrich JD, Young KL, Robinette ML, et al. TREM2 lipid sensing sustains the microglial response in an Alzheimer's disease model. Cell. 2015;160:1061–71.

37. Gjoneska E, Pfenning AR, Mathys H, Quon G, Kundaje A, Tsai L-H, et al. Conserved epigenomic signals in mice and humans reveal immune basis of Alzheimer's disease. Nature. 2015;518:365–9.

38. Karch CM, Goate AM. Alzheimer's disease risk genes and mechanisms of disease pathogenesis. Biol Psychiatry. 2015;77:43–51.

39. Katsumoto A, Takeuchi H, Takahashi K, Tanaka F. Microglia in Alzheimer's Disease: Risk Factors and Inflammation. Front Neurol. 2018;9:978.

40. Guo S, Wang H, Yin Y. Microglia Polarization From M1 to M2 in Neurodegenerative Diseases. Front Aging Neurosci. 2022;14:815347.

41. Shabab T, Khanabdali R, Moghadamtousi SZ, Kadir HA, Mohan G. Neuroinflammation pathways: a general review. Int J Neurosci. 2017;127:624–33.

42. Cherry JD, Olschowka JA, O'Banion MK. Neuroinflammation and M2 microglia: the good, the bad, and the inflamed. J Neuroinflammation. 2014;11:98.

43. Koenigsknecht-Talboo J, Landreth GE. Microglial Phagocytosis Induced by Fibrillar β-Amyloid and IgGs Are Differentially Regulated by Proinflammatory Cytokines. J Neurosci. 2005;25:8240–9.

44. Zhang Y, He M-L. Deferoxamine enhances alternative activation of microglia and inhibits amyloid beta deposits in APP/PS1 mice. Brain Res. 2017;1677:86–92.

45. Saresella M, Marventano I, Calabrese E, Piancone F, Rainone V, Gatti A, et al. A complex proinflammatory role for peripheral monocytes in Alzheimer's disease. J Alzheimers Dis JAD. 2014;38:403–13.

46. Jimenez S, Baglietto-Vargas D, Caballero C, Moreno-Gonzalez I, Torres M, Sanchez-Varo R, et al. Inflammatory response in the hippocampus of PS1M146L/APP751SL mouse model of Alzheimer's disease: age-dependent switch in the microglial phenotype from alternative to classic. J Neurosci Off J Soc Neurosci. 2008;28:11650–61.

47. Varnum MM, Ikezu T. The classification of microglial activation phenotypes on neurodegeneration and regeneration in Alzheimer's disease brain. Arch Immunol Ther Exp (Warsz). 2012;60:251–66.

48. Herber DL, Mercer M, Roth LM, Symmonds K, Maloney J, Wilson N, et al. Microglial activation is required for Abeta clearance after intracranial injection of lipopolysaccharide in APP transgenic mice. J Neuroimmune Pharmacol Off J Soc NeuroImmune Pharmacol. 2007;2:222–31.

49. Majumdar A, Cruz D, Asamoah N, Buxbaum A, Sohar I, Lobel P, et al. Activation of microglia acidifies lysosomes and leads to degradation of Alzheimer amyloid fibrils. Mol Biol Cell. 2007;18:1490–6.

50. Rivera-Escalera F, Pinney JJ, Owlett L, Ahmed H, Thakar J, Olschowka JA, et al. IL-1β-driven amyloid plaque clearance is associated with an expansion of transcriptionally reprogrammed microglia. J Neuroinflammation. 2019;16:261.

51. Shaftel SS, Kyrkanides S, Olschowka JA, Miller JH, Johnson RE, O'Banion MK. Sustained hippocampal IL-1β overexpression mediates chronic neuroinflammation and ameliorates Alzheimer plaque pathology. J Clin Invest. 2007;117:1595–604.

52. Venegas C, Kumar S, Franklin BS, Dierkes T, Brinkschulte R, Tejera D, et al. Microglia-derived ASC specks cross-seed amyloid-β in Alzheimer's disease. Nature. 2017;552:355–61.

53. Ising C, Heneka MT. Functional and structural damage of neurons by innate immune mechanisms during neurodegeneration. Cell Death Dis. 2018;9:1–8.

54. Briddell RA, Hartley CA, Smith KA, McNiece IK. Recombinant Rat Stem Cell Factor Synergizes With Recombinant Human Granulocyte Colony-Stimulating Factor In Vivo in Mice to Mobilize Peripheral Blood Progenitor Cells That Have Enhanced Repopulating Potential. Blood. 1993;82:1720–3.

55. Hess DA, Levac KD, Karanu FN, Rosu-Myles M, White MJ, Gallacher L, et al. Functional analysis of human hematopoietic repopulating cells mobilized with granulocyte colony-stimulating factor alone versus granulocyte colony-stimulating factor in combination with stem cell factor. Blood. 2002;100:869–78.

56. Welte K, Platzer E, Lu L, Gabrilove JL, Levi E, Mertelsmann R, et al. Purification and biochemical characterization of human pluripotent hematopoietic colony-stimulating factor. Proc Natl Acad Sci U S A. 1985;82:1526–30.

57. Zsebo KM, Wypych J, McNiece IK, Lu HS, Smith KA, Karkare SB, et al. Identification, purification, and biological characterization of hematopoietic stem cell factor from buffalo rat liver-conditioned medium. Cell. 1990;63:195–201.

58. Ping S, Qiu X, Kyle M, Hughes K, Longo J, Zhao L-R. Stem cell factor and granulocyte colony-stimulating factor promote brain repair and improve cognitive function through VEGF-A in a mouse model of CADASIL. Neurobiol Dis. 2019;132:104561.

59. Rahi V, Jamwal S, Kumar P. Neuroprotection through G-CSF: recent advances and future viewpoints. Pharmacol Rep PR. 2021;73:372–85.

60. Zhang SC, Fedoroff S. Cellular localization of stem cell factor and c-kit receptor in the mouse nervous system. J Neurosci Res. 1997;47:1–15.

61. Cui L, Murikinati SR, Wang D, Zhang X, Duan W-M, Zhao L-R. Reestablishing neuronal networks in the aged brain by stem cell factor and granulocyte-colony stimulating factor in a mouse model of chronic stroke. PloS One. 2013;8:e64684.

62. Qiu X, Ping S, Kyle M, Chin L, Zhao L-R. Long-term beneficial effects of hematopoietic growth factors on brain repair in the chronic phase of severe traumatic brain injury. Exp Neurol. 2020;330:113335.

63. Ping S, Qiu X, Gonzalez-Toledo ME, Liu X, Zhao L-R. Stem Cell Factor in Combination With Granulocyte Colony-Stimulating Factor Protects the Brain From Capillary Thrombosis-Induced Ischemic Neuron Loss in a Mouse Model of CADASIL. Front Cell Dev Biol. 2020;8:627733.

64. Schneider A, Krüger C, Steigleder T, Weber D, Pitzer C, Laage R, et al. The hematopoietic factor G-CSF is a neuronal ligand that counteracts programmed cell death and drives neurogenesis. J Clin Invest. 2005;115:2083–98.

65. Schneider A, Kuhn H-G, Schäbitz W-R. A role for G-CSF (granulocyte-colony stimulating factor) in the central nervous system. Cell Cycle Georget Tex. 2005;4:1753–7.

66. Su Y, Cui L, Piao C, Li B, Zhao L-R. The effects of hematopoietic growth factors on neurite outgrowth. PloS One. 2013;8:e75562.

67. Tsai K-J, Tsai Y-C, Shen C-KJ. G-CSF rescues the memory impairment of animal models of Alzheimer's disease. J Exp Med. 2007;204:1273–80.

68. Barber RC, Edwards MI, Xiao G, Huebinger RM, Diaz-Arrastia R, Wilhelmsen KC, et al. Serum Granulocyte Colony-Stimulating Factor and Alzheimer's Disease. Dement Geriatr Cogn Disord EXTRA. 2012;2:353–60.

69. Laske C, Sopova K, Hoffmann N, Stransky E, Hagen K, Fallgatter AJ, et al. Stem cell factor plasma levels are decreased in Alzheimer's disease patients with fast cognitive decline after one-year follow-up period: the Pythia-study. J Alzheimers Dis JAD. 2011;26:39–45.

70. Laske C, Stellos K, Stransky E, Seizer P, Akcay O, Eschweiler GW, et al. Decreased plasma and cerebrospinal fluid levels of stem cell factor in patients with early Alzheimer's disease. J Alzheimers Dis JAD. 2008;15:451–60.

71. Laske C, Stellos K, Stransky E, Leyhe T, Gawaz M. Decreased plasma levels of granulocyte-colony stimulating factor (G-CSF) in patients with early Alzheimer's disease. J Alzheimers Dis JAD. 2009;17:115–23.

72. Li B, Gonzalez-Toledo ME, Piao C-S, Gu A, Kelley RE, Zhao L-R. Stem cell factor and granulocyte colony-stimulating factor reduce β-amyloid deposits in the brains of APP/PS1 transgenic mice. Alzheimers Res Ther. 2011;3:8.

73. Jiang H, Liu CX, Feng JB, Wang P, Zhao CP, Xie ZH, et al. Granulocyte colony-stimulating factor attenuates chronic neuroinflammation in the brain of amyloid precursor protein transgenic mice: an Alzheimer's disease mouse model. J Int Med Res. 2010;38:1305–12.

74. Sanchez-Ramos J, Song S, Sava V, Catlow B, Lin X, Mori T, et al. Granulocyte Colony Stimulating Factor (G-CSF) Decreases Brain Amyloid Burden and Reverses Cognitive Impairment in Alzheimer's Mice. Neuroscience. 2009;163:55–72.

75. Terashima T, Nakae Y, Katagi M, Okano J, Suzuki Y, Kojima H. Stem cell factor induces polarization of microglia to the neuroprotective phenotype in vitro. Heliyon. 2018;4:e00837.

76. Keren-Shaul H, Spinrad A, Weiner A, Matcovitch-Natan O, Dvir-Szternfeld R, Ulland TK, et al. A Unique Microglia Type Associated with Restricting Development of Alzheimer's Disease. Cell. 2017;169:1276-1290.e17.

77. Lee S-H, Meilandt WJ, Xie L, Gandham VD, Ngu H, Barck KH, et al. Trem2 restrains the enhancement of tau accumulation and neurodegeneration by β-amyloid pathology. Neuron. 2021;109:1283-1301.e6.

78. Jankowsky JL, Fadale DJ, Anderson J, Xu GM, Gonzales V, Jenkins NA, et al. Mutant presenilins specifically elevate the levels of the 42 residue beta-amyloid peptide in vivo: evidence for augmentation of a 42-specific gamma secretase. Hum Mol Genet. 2004;13:159–70.

79. Ekiz HA, Conley CJ, Stephens WZ, O'Connell RM. CIPR: a web-based R/shiny app and R package to annotate cell clusters in single cell RNA sequencing experiments. BMC Bioinformatics. 2020;21:191.

80. Heng TSP, Painter MW, Immunological Genome Project Consortium. The Immunological Genome Project: networks of gene expression in immune cells. Nat Immunol. 2008;9:1091–4.

81. Benjamini Y, Hochberg Y. Controlling the False Discovery Rate: A Practical and Powerful Approach to Multiple Testing. J R Stat Soc Ser B Methodol. 1995;57:289–300.

82. Goedhart J, Luijsterburg MS. VolcaNoseR is a web app for creating, exploring, labeling and sharing volcano plots. Sci Rep. 2020;10:20560.

83. Doncheva NT, Morris JH, Gorodkin J, Jensen LJ. Cytoscape StringApp: Network Analysis and Visualization of Proteomics Data. J Proteome Res. 2019;18:623–32.

84. Shannon P, Markiel A, Ozier O, Baliga NS, Wang JT, Ramage D, et al. Cytoscape: a software environment for integrated models of biomolecular interaction networks. Genome Res. 2003;13:2498–504.

85. Haage V, Semtner M, Vidal RO, Hernandez DP, Pong WW, Chen Z, et al. Comprehensive gene expression meta-analysis identifies signature genes that distinguish microglia from peripheral monocytes/macrophages in health and glioma. Acta Neuropathol Commun. 2019;7:20.

86. Hohsfield LA, Tsourmas KI, Ghorbanian Y, Syage AR, Jin Kim S, Cheng Y, et al. MAC2 is a long-lasting marker of peripheral cell infiltrates into the mouse CNS after bone marrow transplantation and coronavirus infection. Glia. 2022;70:875–91.

87. McFarland HI, Nahill SR, Maciaszek JW, Welsh RM. CD11b (Mac-1): a marker for CD8+ cytotoxic T cell activation and memory in virus infection. J Immunol Baltim Md 1950. 1992;149:1326–33.

88. Butovsky O, Weiner HL. Microglial signatures and their role in health and disease. Nat Rev Neurosci. 2018;19:622–35.

89. Deczkowska A, Keren-Shaul H, Weiner A, Colonna M, Schwartz M, Amit I. Disease-Associated Microglia: A Universal Immune Sensor of Neurodegeneration. Cell. 2018;173:1073–81.

90. Rangaraju S, Dammer EB, Raza SA, Rathakrishnan P, Xiao H, Gao T, et al. Identification and therapeutic modulation of a pro-inflammatory subset of disease-associated-microglia in Alzheimer's disease. Mol Neurodegener. 2018;13:24.

91. Zhang GX, Li J, Ventura E, Rostami A. Parenchymal microglia of naïve adult C57BL/6J mice express high levels of B7.1, B7.2, and MHC class II. Exp Mol Pathol. 2002;73:35–45.

92. Ford AL, Goodsall AL, Hickey WF, Sedgwick JD. Normal adult ramified microglia separated from other central nervous system macrophages by flow cytometric sorting. Phenotypic differences defined and direct ex vivo antigen presentation to myelin basic protein-reactive CD4+ T cells compared. J Immunol Baltim Md 1950. 1995;154:4309–21.

93. Cristóvão JS, Gomes CM. S100 Proteins in Alzheimer's Disease. Front Neurosci. 2019;13:463.

94. Kummer MP, Vogl T, Axt D, Griep A, Vieira-Saecker A, Jessen F, et al. Mrp14 deficiency ameliorates amyloid β burden by increasing microglial phagocytosis and modulation of amyloid precursor protein processing. J Neurosci Off J Soc Neurosci. 2012;32:17824–9.

95. Grabert K, Michoel T, Karavolos MH, Clohisey S, Baillie JK, Stevens MP, et al. Microglial brain region-dependent diversity and selective regional sensitivities to aging. Nat Neurosci. 2016;19:504–16.

96. Chen Y, Colonna M. Microglia in Alzheimer's disease at single-cell level. Are there common patterns in humans and mice? J Exp Med. 2021;218:e20202717.

97. Hammond TR, Dufort C, Dissing-Olesen L, Giera S, Young A, Wysoker A, et al. Single-Cell RNA Sequencing of Microglia throughout the Mouse Lifespan and in the Injured Brain Reveals Complex Cell-State Changes. Immunity. 2019;50:253-271.e6.

98. Orre M, Kamphuis W, Osborn LM, Melief J, Kooijman L, Huitinga I, et al. Acute isolation and transcriptome characterization of cortical astrocytes and microglia from young and aged mice. Neurobiol Aging. 2014;35:1–14.

99. Wang H. Microglia Heterogeneity in Alzheimer's Disease: Insights From Single-Cell Technologies. Front Synaptic Neurosci [Internet]. 2021 [cited 2022 Dec 17];13. Available from: https://www.frontiersin.org/articles/10.3389/fnsyn.2021.773590

100. Kenkhuis B, Somarakis A, Kleindouwel LRT, van Roon-Mom WMC, Höllt T, van der Weerd L. Co-expression patterns of microglia markers Iba1, TMEM119 and P2RY12 in Alzheimer's disease. Neurobiol Dis. 2022;167:105684.

101. Grassivaro F, Menon R, Acquaviva M, Ottoboni L, Ruffini F, Bergamaschi A, et al. Convergence between Microglia and Peripheral Macrophages Phenotype during Development and Neuroinflammation. J Neurosci. 2020;40:784–95.

102. Audrain M, Haure-Mirande J-V, Mleczko J, Wang M, Griffin JK, St George-Hyslop PH, et al. Reactive or transgenic increase in microglial TYROBP reveals a TREM2-independent TYROBP-APOE link in wild-type and Alzheimer's-related mice. Alzheimers Dement J Alzheimers Assoc. 2021;17:149–63.

103. Grubman A, Choo XY, Chew G, Ouyang JF, Sun G, Croft NP, et al. Transcriptional signature in microglia associated with Aβ plaque phagocytosis. Nat Commun. 2021;12:3015.

104. Wang S, Song R, Wang Z, Jing Z, Wang S, Ma J. S100A8/A9 in Inflammation. Front Immunol [Internet]. 2018 [cited 2022 Dec 8];9. Available from: https://www.frontiersin.org/articles/10.3389/fimmu.2018.01298

105. Gong Y, Hart E, Shchurin A, Hoover-Plow J. Inflammatory macrophage migration requires MMP-9 activation by plasminogen in mice. J Clin Invest. 2008;118:3012–24.

106. Gross SR, Sin CGT, Barraclough R, Rudland PS. Joining S100 proteins and migration: for better or for worse, in sickness and in health. Cell Mol Life Sci CMLS. 2014;71:1551–79.

107. Jang E, Lee S, Kim J-H, Kim J-H, Seo J-W, Lee W-H, et al. Secreted protein lipocalin-2 promotes microglial M1 polarization. FASEB J Off Publ Fed Am Soc Exp Biol. 2013;27:1176–90.

108. Kang H, Shin HJ, An HS, Jin Z, Lee JY, Lee J, et al. Role of Lipocalin-2 in Amyloid-Beta Oligomer-Induced Mouse Model of Alzheimer's Disease. Antioxid Basel Switz. 2021;10:1657.

109. Lee S, Kim J-H, Kim J-H, Seo J-W, Han H-S, Lee W-H, et al. Lipocalin-2 Is a chemokine inducer in the central nervous system: role of chemokine ligand 10 (CXCL10) in lipocalin-2-induced cell migration. J Biol Chem. 2011;286:43855–70.

110. Ehrchen JM, Sunderkötter C, Foell D, Vogl T, Roth J. The endogenous Toll–like receptor 4 agonist S100A8/S100A9 (calprotectin) as innate amplifier of infection, autoimmunity, and cancer. J Leukoc Biol. 2009;86:557–66.

111. He Z, Riva M, Björk P, Swärd K, Mörgelin M, Leanderson T, et al. CD14 Is a Co-Receptor for TLR4 in the S100A9-Induced Pro-Inflammatory Response in Monocytes. PLoS ONE. 2016;11:e0156377.

112. Vogl T, Ludwig S, Goebeler M, Strey A, Thorey IS, Reichelt R, et al. MRP8 and MRP14 control microtubule reorganization during transendothelial migration of phagocytes. Blood. 2004;104:4260–8.

113. Chang K-A, Kim HJ, Suh Y-H. The role of S100a9 in the pathogenesis of Alzheimer's disease: the therapeutic effects of S100a9 knockdown or knockout. Neurodegener Dis. 2012;10:27–9.

114. Pansieri J, Iashchishyn IA, Fakhouri H, Ostojić L, Malisauskas M, Musteikyte G, et al. Templating S100A9 amyloids on Aβ fibrillar surfaces revealed by charge detection mass spectrometry, microscopy, kinetic and microfluidic analyses. Chem Sci. 2020;11:7031–9.

115. Wang C, Klechikov AG, Gharibyan AL, Wärmländer SKTS, Jarvet J, Zhao L, et al. The role of pro-inflammatory S100A9 in Alzheimer's disease amyloid-neuroinflammatory cascade. Acta Neuropathol (Berl). 2014;127:507–22.

116. Russo A, Schürmann H, Brandt M, Scholz K, Matos ALL, Grill D, et al. Alarming and Calming: Opposing Roles of S100A8/S100A9 Dimers and Tetramers on Monocytes. Adv Sci Weinh Baden-Wurtt Ger. 2022;e2201505.

117. Otsuka K, Terasaki F, Ikemoto M, Fujita S, Tsukada B, Katashima T, et al. Suppression of inflammation in rat autoimmune myocarditis by S100A8/A9 through modulation of the proinflammatory cytokine network. Eur J Heart Fail. 2009;11:229–37.

118. Karlstetter M, Walczak Y, Weigelt K, Ebert S, Van den Brulle J, Schwer H, et al. The novel activated microglia/macrophage WAP domain protein, AMWAP, acts as a counter-regulator of proinflammatory response. J Immunol Baltim Md 1950. 2010;185:3379–90.

119. Camilli C, Hoeh AE, De Rossi G, Moss SE, Greenwood J. LRG1: an emerging player in disease pathogenesis. J Biomed Sci. 2022;29:6.

120. Ikeda N, Asano K, Kikuchi K, Uchida Y, Ikegami H, Takagi R, et al. Emergence of immunoregulatory Ym1+Ly6Chi monocytes during recovery phase of tissue injury. Sci Immunol. 2018;3:eaat0207.

121. Kang Q, Li L, Pang Y, Zhu W, Meng L. An update on Ym1 and its immunoregulatory role in diseases. Front Immunol [Internet]. 2022 [cited 2023 Jan 1];13. Available from: https://www.frontiersin.org/articles/10.3389/fimmu.2022.891220

122. Liu K, Tian L-X, Tang X, Wang J, Tang W-Q, Ma Z-F, et al. Neutrophilic granule protein (NGP) attenuates lipopolysaccharide-induced inflammatory responses and enhances phagocytosis of bacteria by macrophages. Cytokine. 2020;128:155001.

123. Makita N, Hizukuri Y, Yamashiro K, Murakawa M, Hayashi Y. IL-10 enhances the phenotype of M2 macrophages induced by IL-4 and confers the ability to increase eosinophil migration. Int Immunol. 2015;27:131–41.

124. Liu N, Jiang Y, Chung JY, Li Y, Yu Z, Kim JW, et al. Annexin A2 Deficiency Exacerbates Neuroinflammation and Long-Term Neurological Deficits after Traumatic Brain Injury in Mice. Int J Mol Sci. 2019;20:6125.

125. Morimoto M, Nakano T, Egashira S, Irie K, Matsuyama K, Wada M, et al. Haptoglobin Regulates Macrophage/Microglia-Induced Inflammation and Prevents Ischemic Brain Damage Via Binding to HMGB1. J Am Heart Assoc. 2022;11:e024424.

126. McArthur S, Cristante E, Paterno M, Christian H, Roncaroli F, Gillies GE, et al. Annexin A1: a central player in the anti-inflammatory and neuroprotective role of microglia. J Immunol Baltim Md 1950. 2010;185:6317–28.

127. Aslanidis A, Karlstetter M, Scholz R, Fauser S, Neumann H, Fried C, et al. Activated microglia/macrophage whey acidic protein (AMWAP) inhibits NFκB signaling and induces a neuroprotective phenotype in microglia. J Neuroinflammation. 2015;12:77.

128. Ries M, Loiola R, Shah UN, Gentleman SM, Solito E, Sastre M. The anti-inflammatory Annexin A1 induces the clearance and degradation of the amyloid-β peptide. J Neuroinflammation. 2016;13:234.

129. Ries M, Watts H, Mota BC, Lopez MY, Donat CK, Baxan N, et al. Annexin A1 restores cerebrovascular integrity concomitant with reduced amyloid-β and tau pathology. Brain J Neurol. 2021;144:1526–41.

130. Xia Q, Li X, Zhou H, Zheng L, Shi J. S100A11 protects against neuronal cell apoptosis induced by cerebral ischemia via inhibiting the nuclear translocation of annexin A1. Cell Death Dis. 2018;9:657.

131. Tian Z-Y, Wang C-Y, Wang T, Li Y-C, Wang Z-Y. Glial S100A6 Degrades β-amyloid Aggregation through Targeting Competition with Zinc Ions. Aging Dis. 2019;10:756–69.

132. Garland P, Morton MJ, Haskins W, Zolnourian A, Durnford A, Gaastra B, et al. Haemoglobin causes neuronal damage in vivo which is preventable by haptoglobin. Brain Commun. 2020;2:fcz053.

133. Graff-Radford J, Lesnick T, Rabinstein AA, Gunter J, Aakre J, Przybelski SA, et al. Cerebral microbleed incidence, relationship to amyloid burden: The Mayo Clinic Study of Aging. Neurology. 2020;94:e190–9.

134. Yerbury JJ, Kumita JR, Meehan S, Dobson CM, Wilson MR. α2-Macroglobulin and Haptoglobin Suppress Amyloid Formation by Interacting with Prefibrillar Protein Species *. J Biol Chem. 2009;284:4246–54.

135. Paudel YN, Angelopoulou E, Piperi C, Othman I, Aamir K, Shaikh MF. Impact of HMGB1, RAGE, and TLR4 in Alzheimer's Disease (AD): From Risk Factors to Therapeutic Targeting. Cells. 2020;9:383.

136. Takata K, Kitamura Y, Tsuchiya D, Kawasaki T, Taniguchi T, Shimohama S. High mobility group box protein-1 inhibits microglial Abeta clearance and enhances Abeta neurotoxicity. J Neurosci Res. 2004;78:880–91.

137. Vafadari B, Salamian A, Kaczmarek L. MMP-9 in translation: from molecule to brain physiology, pathology, and therapy. J Neurochem. 2016;139:91–114.

138. Miners JS, Baig S, Palmer J, Palmer LE, Kehoe PG, Love S. Abeta-degrading enzymes in Alzheimer's disease. Brain Pathol Zurich Switz. 2008;18:240–52.

139. Yan P, Hu X, Song H, Yin K, Bateman RJ, Cirrito JR, et al. Matrix metalloproteinase-9 degrades amyloid-beta fibrils in vitro and compact plaques in situ. J Biol Chem. 2006;281:24566–74.

140. Fragkouli A, Tsilibary EC, Tzinia AK. Neuroprotective role of MMP-9 overexpression in the brain of Alzheimer's 5xFAD mice. Neurobiol Dis. 2014;70:179–89.

141. Dar NJ, Glazner GW. Deciphering the neuroprotective and neurogenic potential of soluble amyloid precursor protein alpha (sAPPα). Cell Mol Life Sci CMLS. 2020;77:2315–30.

142. Mockett BG, Richter M, Abraham WC, Müller UC. Therapeutic Potential of Secreted Amyloid Precursor Protein APPsα. Front Mol Neurosci. 2017;10:30.

143. Das N, Raymick J, Sarkar S. Role of metals in Alzheimer's disease. Metab Brain Dis. 2021;36:1627–39.

144. Wang L, Yin Y-L, Liu X-Z, Shen P, Zheng Y-G, Lan X-R, et al. Current understanding of metal ions in the pathogenesis of Alzheimer's disease. Transl Neurodegener. 2020;9:10.

145. Hunter M, Spiller KJ, Dominique MA, Xu H, Hunter FW, Fang TC, et al. Microglial transcriptome analysis in the rNLS8 mouse model of TDP-43 proteinopathy reveals discrete expression profiles associated with neurodegenerative progression and recovery. Acta Neuropathol Commun. 2021;9:140.

146. Smyth L, Murray H, Hill M, Leeuwen E, Highet B, Magon N, et al. Neutrophil-vascular interactions drive myeloperoxidase accumulation in the brain in Alzheimer's disease. Acta Neuropathol Commun. 2022;10.

147. Zenaro E, Pietronigro E, Bianca VD, Piacentino G, Marongiu L, Budui S, et al. Neutrophils promote Alzheimer's disease–like pathology and cognitive decline via LFA-1 integrin. Nat Med. 2015;21:880–6.

148. Meyer-Luehmann M, Prinz M. Myeloid cells in Alzheimer's disease: culprits, victims or innocent bystanders? Trends Neurosci. 2015;38:659–68.

149. Gordon B, Blazey T, Benzinger T. Regional variability in Alzheimer's disease biomarkers. Future Neurol. 2014;9:131–4.